6
Some Nonlinear Problems

6.1 Kinematics

Recall from Sect. 2.5 of Chap. 2 that displacements alone cannot be related effectively to stresses to describe material behavior. Rather, combinations of displacement gradients, called strains, are more useful in formulating constitutive equations for stress. Indeed, in Eq. (2.42), we listed six independent components of the Green strain, which is an exact measure for large or small deformations that is insensitive to rigid-body motions. There is, however, a more fundamental measure of motion that is useful in large deformation problems; it is called the *deformation gradient*. Recall, therefore, that we said the displacement vector $\boldsymbol{u}$ is a measure of where we (a material particle) are minus where we were. In Cartesian coordinates, we have the following three components

$$u_x = x(X,Y,Z) - X, \quad u_y = y(X,Y,Z) - Y, \quad u_z = z(X,Y,Z) - Z, \tag{6.1}$$

where (x, y, z) locates a point of interest in the current configuration and (X, Y, Z) locates the same point in its original (reference) configuration. In particular, it is because the location of a point in a current configuration depends on where it started that we need the functional dependence $x(X, Y, Z)$, and so too for y and z. Moreover, the displacement gradients can be written

$$\frac{\partial u_x}{\partial X} = \frac{\partial x}{\partial X} - 1, \quad \frac{\partial u_y}{\partial Y} = \frac{\partial y}{\partial Y} - 1, \quad \frac{\partial u_z}{\partial Z} = \frac{\partial z}{\partial Z} - 1, \tag{6.2}$$

J.D. Humphrey, S.L. O'Rourke, *An Introduction to Biomechanics*,
DOI 10.1007/978-1-4939-2623-7_6

and so forth. Given that there are nine such terms, it is convenient to write these results in a matrix form.[1] Indeed, if we denote the displacement gradient matrix by $[H]$ and the deformation gradient matrix by $[F]$, then we see that

$$[H] = [F] - [I] \leftrightarrow [F] = [I] + [H], \tag{6.3}$$

where the components of the deformation gradient can be calculated (with respect to Cartesian coordinates) via

$$[F] = \begin{bmatrix} \frac{\partial x}{\partial X} & \frac{\partial x}{\partial Y} & \frac{\partial x}{\partial Z} \\ \frac{\partial y}{\partial X} & \frac{\partial y}{\partial Y} & \frac{\partial y}{\partial Z} \\ \frac{\partial z}{\partial X} & \frac{\partial z}{\partial Y} & \frac{\partial z}{\partial Z} \end{bmatrix}. \tag{6.4}$$

$[I]$ is the so-called identity matrix, with components

$$[I] = \begin{bmatrix} 1 & 0 & 0 \\ 0 & 1 & 0 \\ 0 & 0 & 1 \end{bmatrix}. \tag{6.5}$$

This matrix is called an identity matrix for $[A][I] = [I][A] = [A]$ for any 3×3 matrix $[A]$; that is, when $[I]$ operates on a matrix $[A]$, it returns $[A]$ unaltered.

It is the deformation gradient that plays the key role in nonlinear analyses—it is the fundamental measure of finite deformation for it includes both the deformation and the rigid-body motion. For example, if we denote the Green strain via the matrix $[E]$, where

$$[E] = \begin{bmatrix} E_{XX} & E_{XY} & E_{XZ} \\ E_{YX} & E_{YY} & E_{YZ} \\ E_{ZX} & E_{ZY} & E_{ZZ} \end{bmatrix} \tag{6.6}$$

are the Cartesian components that are listed in Eq. (2.42), it is easy to show that

$$[E] = \frac{1}{2}\Big([F]^T[F] - [I]\Big), \tag{6.7}$$

where the superscript T denotes a transpose of the matrix (i.e., the interchanging of rows and columns as discussed in Appendix 6). Without going into details (see Humphrey 2002), the operation of $[F]^T[F]$ removes the rigid-body

[1] Matrix operations are reviewed briefly in Appendix 6.

information and the subtraction of $[I]$ renders $[E]=[0]$ in the absence of deformation/strain; both of these features are desirable of a strain measure. It can be shown further that the linearized strain is given by

$$[\varepsilon]=\frac{1}{2}\Big([F]+[F]^T-2[I]\Big). \tag{6.8}$$

Example 6.1 Compute the components of $[F]$ for the motions associated with Eqs. (2.50), (2.52), and (2.55), and then calculate the associated values of $[E]$ and $[\varepsilon]$.

Solution: First, consider the mathematically simple 1-D stretching motion given by $x=\Lambda X$, $y=Y$, and $z=Z$, where Λ is a stretch ratio (i.e., just a number for each equilibrium stretch). Clearly,

$$[F]=\begin{bmatrix} \frac{\partial x}{\partial X} & \frac{\partial x}{\partial Y} & \frac{\partial x}{\partial Z} \\ \frac{\partial y}{\partial X} & \frac{\partial y}{\partial Y} & \frac{\partial y}{\partial Z} \\ \frac{\partial z}{\partial X} & \frac{\partial z}{\partial Y} & \frac{\partial z}{\partial Z} \end{bmatrix}=\begin{bmatrix} \Lambda & 0 & 0 \\ 0 & 1 & 0 \\ 0 & 0 & 1 \end{bmatrix}$$

and therefore

$$[E]=\frac{1}{2}\Big([F]^T[F]-[I]\Big)=\begin{bmatrix} \frac{1}{2}(\Lambda^2-1) & 0 & 0 \\ 0 & 0 & 0 \\ 0 & 0 & 0 \end{bmatrix},$$

whereas

$$[\varepsilon]=\frac{1}{2}\Big([F]+[F]^T-2[I]\Big)=\begin{bmatrix} \Lambda-1 & 0 & 0 \\ 0 & 0 & 0 \\ 0 & 0 & 0 \end{bmatrix},$$

as we found earlier. Again, for $\Lambda\sim 1$ (small strain), the numerical values of $[E]$ and $[\varepsilon]$ differ little, but for larger values typically experienced by soft tissues (stretches often on the order of 10–100 %), the difference becomes pronounced. For example, if $\Lambda=1.5$, a 50 % extension, then $E_{11}=0.625$ (exact) and $\varepsilon_{11}=0.5$ (approximate), thus revealing a 20 % error in the computation of the strain. Question: Why would this motion be difficult to achieve in the lab?

Second, consider a simple shear motion given by $x = X + \kappa Y$, $y = Y$, and $z = Z$, where κ is just a number for each equilibrium motion. Hence,

$$[F] = \begin{bmatrix} 1 & \kappa & 0 \\ 0 & 1 & 0 \\ 0 & 0 & 1 \end{bmatrix}$$

and, therefore,

$$[E] = \frac{1}{2}\left(\begin{bmatrix} 1 & 0 & 0 \\ \kappa & 1 & 0 \\ 0 & 0 & 1 \end{bmatrix} \begin{bmatrix} 1 & \kappa & 0 \\ 0 & 1 & 0 \\ 0 & 0 & 1 \end{bmatrix} - \begin{bmatrix} 1 & 0 & 0 \\ 0 & 1 & 0 \\ 0 & 0 & 1 \end{bmatrix} \right) = \frac{1}{2} \begin{bmatrix} 0 & \kappa & 0 \\ \kappa & \kappa^2 & 0 \\ 0 & 0 & 0 \end{bmatrix},$$

whereas

$$[\varepsilon] = \frac{1}{2}\left(\begin{bmatrix} 1 & \kappa & 0 \\ 0 & 1 & 0 \\ 0 & 0 & 1 \end{bmatrix} + \begin{bmatrix} 1 & 0 & 0 \\ \kappa & 1 & 0 \\ 0 & 0 & 1 \end{bmatrix} - \begin{bmatrix} 2 & 0 & 0 \\ 0 & 2 & 0 \\ 0 & 0 & 2 \end{bmatrix} \right) = \frac{1}{2} \begin{bmatrix} 0 & \kappa & 0 \\ \kappa & 0 & 0 \\ 0 & 0 & 0 \end{bmatrix}.$$

This comparison reveals a significant conceptual difference between $[E]$ and $[\varepsilon]$. Note that the extensional strain in the Y direction $E_{YY} = \kappa^2/2$ whereas $\varepsilon_{yy} = 0$; that is, shear and extension are coupled in the (exact) nonlinear theory, whereas the linearization of $[\varepsilon]$ loses this coupling. Although $\kappa^2/2$ will be negligible in comparison to $\kappa/2$ if $\kappa \ll 1$, this will not be the case for large shears, as experienced by the heart during each cardiac cycle. Again, therefore, the exact (nonlinear) theory must be used when the deformations or rigid rotations are large. The latter is revealed by considering the third case, the rigid-body motion associated with Eq. (2.55):

$$x = X\cos\phi + Y\sin\phi, \quad y = -X\sin\phi + Y\cos\phi, \quad z = Z.$$

In this case,

$$[E] = \frac{1}{2}\left(\begin{bmatrix} \cos\phi & -\sin\phi & 0 \\ \sin\phi & \cos\phi & 0 \\ 0 & 0 & 1 \end{bmatrix} \begin{bmatrix} \cos\phi & \sin\phi & 0 \\ -\sin\phi & \cos\phi & 0 \\ 0 & 0 & 1 \end{bmatrix} - \begin{bmatrix} 1 & 0 & 0 \\ 0 & 1 & 0 \\ 0 & 0 & 1 \end{bmatrix} \right)$$
$$= \begin{bmatrix} 0 & 0 & 0 \\ 0 & 0 & 0 \\ 0 & 0 & 0 \end{bmatrix},$$

as it should, for $[E]$ is insensitive to rigid-body motion, but

$$[\varepsilon] = \frac{1}{2}\left(\begin{bmatrix} \cos\phi & \sin\phi & 0 \\ -\sin\phi & \cos\phi & 0 \\ 0 & 0 & 1 \end{bmatrix} + \begin{bmatrix} \cos\phi & -\sin\phi & 0 \\ \sin\phi & \cos\phi & 0 \\ 0 & 0 & 1 \end{bmatrix} - \begin{bmatrix} 2 & 0 & 0 \\ 0 & 2 & 0 \\ 0 & 0 & 2 \end{bmatrix}\right)$$
$$= \begin{bmatrix} \cos\phi - 1 & 0 & 0 \\ 0 & \cos\phi - 1 & 0 \\ 0 & 0 & 0 \end{bmatrix},$$

as found in Eq. (2.56), which reveals that $[\varepsilon]$ is inappropriately sensitive to a rigid-body rotation unless the rotation is small (i.e., as $\phi \to 0$, $\cos\ \phi \to 1$). Although these three motions are very simple, they serve to illustrate the use of $[F]$ as a fundamental measure of the motion.

Observation 6.1. The cell is the fundamental structural and functional unit of living things and, as noted in Chap. 1, understanding mechanotransduction therein is vital to many areas of biomechanical analysis and design. As one might expect, many different types of tests have been performed on cells in an attempt to correlate changes in cell structure and function with mechanical stimuli. These tests include micropipette aspiration, indentation tests, atomic force microscopy (AFM, both indentation and pulling), and magnetic bead cytometry (Fig. 6.1). In micropipette aspiration, one infers the bending stiffness of the cell membrane by monitoring the amount of cell membrane that is drawn into a pipette of known radius by a known pressure gradient. In indentation tests, one measures the force that is required to indent the cell a known amount and interprets this relation in terms of homogenized properties of the cell membrane and cytoplasm. The AFM was discussed in Chap. 5. One can use

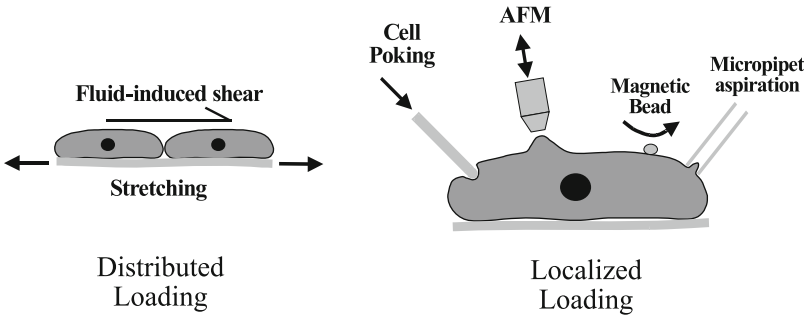

FIGURE 6.1 Possible tests for interrogating the mechanical properties or responses of cells. Micropipette aspiration, magnetic bead cytometry, atomic force microscopy (AFM), and cell poking induce localized loads, whereas stretching sheets on which cells are adhered or subjecting a monolayer of cells to a fluid-flow-induced shear stress induce distributed loads. Flow-induced shears are discussed in Chap. 9 on biofluid mechanics. (Courtesy of R. Gleason).

the AFM to indent the cell or to pull on focal adhesion complexes by functionalizing the tip of the AFM with an appropriate ligand. In magnetic bead cytometry, one similarly functionalizes a magnetic microsphere that can be moved within a magnetic field and then measures torque–twist responses, often over small twists. This test is thus useful for interrogating time-dependent shearing (viscoelastic) behaviors, which are discussed in Chap. 11. Clearly, therefore, advances in technology permit such empirical studies to be performed, but the interpretation of the data requires a biomechanical analysis of the associated initial boundary value problem. Given the complex geometries and loading, many in cell mechanics have assumed linear material behaviors and small strains to facilitate analysis. Such assumptions should be based on the physics, however, not the ease of solution, and the experiments should be designed based on theoretical frameworks, not just the availability of a new technology.

Associated with these many experiments has been a variety of attempts to model the mechanics of cells. Among various models, one finds the following: tensegrity models, which emphasize the importance of prestress within a cell and the possibility of mechanical stresses acting at a distance; percolation theories that emphasize dynamic changes in cytoskeletal interconnectiveness; soft glassy rheological models that suggest that the cytoskeleton is metastable, able to transform instantaneously from more solid-like to more fluid-like behaviors; and continuum models, based on cells as inclusions within a matrix that allow study of cell–matrix interactions (see Mow et al. 1994; Stamenovic and Ingber 2002; Humphrey 2002 and references therein). No single model enjoys wide acceptance, however, even for a particular class of mechanocytes; thus, there remains a pressing need for much more research on cell mechanics. Cell mechanics is essential, for example, for explaining basic processes such as cell adhesion, contraction, division, migration, spreading, and even phagocytosis (the engulfing and digestion of extracellular material). Likewise, it appears that cellular apoptosis (i.e., programmed cell death), the synthesis and degradation of matrix, and the production of growth regulatory molecules, cytokines, and cell surface receptors are also influenced greatly by the mechanics. Each of these activities manifests itself at the tissue and organ level, of course, and thereby are linked to development, tissue maintenance, wound healing, growth and remodeling, and pathogenesis. Hence, whether one seeks to understand normal physiology, disease, injury, interactions between medical devices and tissues, or even the engineering of tissue or organ replacements, there is a need to understand the mechanics of cells. Given the diversity of cell types and the various environments in which they function, we should probably expect that multiple approaches will be equally useful in modeling the many different

aspects of cell mechanics. Although not emphasized in the past, *large strain analyses must be used to describe well the finite displacement gradients and finite rotations experienced by the cell membrane and cytoskeletal constituents*, which together endow the cell with much of its structural integrity. The interested reader is referred to the collection of papers in Mow et al. (1994) and a special issue of the *Journal of Biomechanics* (Vol. 28, pp. 1411–1572, 1995) for a discussion of some of these issues.

6.2 Pseudoelastic Constitutive Relations

Figure 6.2 shows a typical 1-D stress–stretch behavior of a soft tissue. As in Chap. 2, note the nonlinear response, which is initially compliant but then becomes very stiff, and the hysteresis, which reveals an inelastic character. Although the exact source of the inelasticity is not clear, it is thought to be due in part to the movement of structural proteins (primarily elastin and types I and III collagen) within the so-called ground substance matrix that consists largely of proteoglycans and water; that is, one source of energy dissipation revealed by the noncoincident loading and unloading curves may be a viscous dissipation and, in particular, a solid–fluid interaction at the molecular level. We will briefly discuss approaches to model *viscoelastic* responses in Chap. 11, but let us make a further observation here.

Most viscoelastic responses depend not just on the amount of the deformation but also the rate of deformation. A very simple example of this is revealed by a "kindergarten experiment." If one pulls his or her fingers very slowly through a solution of cornstarch (a solid–fluid mixture), the resistance is very small; in contrast, if the fingers are pulled through rapidly, the resistance increases considerably. That is, the response by the cornstarch solution to the applied load depends strongly on the rate of deformation, a characteristic common for

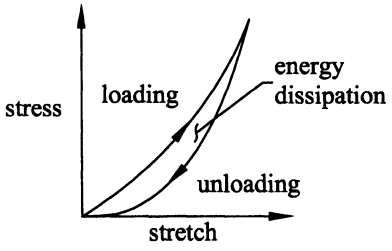

FIGURE 6.2 Typical stress–stretch response of a soft tissue. The nonlinear behavior is usually over finite strains, which disallows the use of Hooke's law and linearized strains, and thus necessitates the formulation of more general constitutive relations Note, too, that the hysteresis is a characteristic of a viscoelastic behavior, or perhaps if small, a pseudoelastic behavior as defined by Y.C. Fung.

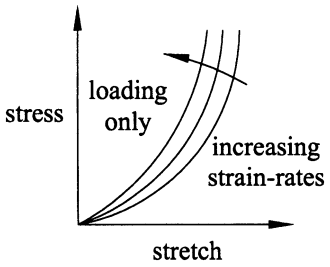

FIGURE 6.3 Possible sensitivity of the stress–stretch response to changes in strain rate (loading curves only). In many cases, however, there is little change in the response with three orders of magnitude changes in strain rate.

viscoelastic behavior (discussed more in Chap. 7). Although most soft tissues exhibit a viscoelastic character under many conditions, Fung reported in the late 1960s that the behavior of soft tissues tends not to depend strongly on strain rate (Fig. 6.3) (see Fung 1990). Indeed, Fung suggested that if one cyclically loads and unloads various soft tissues, there tends to be repeatable (but separate) loading and unloading responses. Because the theory of viscoelasticity is more complex to implement than is the theory of elasticity, Fung suggested that in some cases it may be reasonable to treat separately the loading and unloading behaviors as elastic; that is, although one would use the same function to relate stress to strain in loading and unloading, one would use separate values of the associated material parameters. To remind us that the behavior is not truly elastic, Fung called such an approach *pseudoelasticity*, which is now used frequently in many areas of biomechanical design and analysis.

At this juncture, let us note that Fung's concept of pseudoelasticity appears to be particularly applicable to tissues that are subjected in vivo to consistent loading and unloading, such as the arteries, diastolic heart, and lungs. Indeed, Fung also showed that pseudoelastic responses (i.e., separate but repeatable loading and unloading behaviors) were obtained in the laboratory only after a sufficient number of loading cycles (Fig. 6.4), usually 3–10; that is, it appears that following excision, whereby the tissue is removed from its normal dynamic loading environment, the tissue must be "conditioned" to obtain a repeatable pseudoelastic response. Given such conditioning, the tissue tends to dissipate less energy upon cyclic loading and to become less stiff, both of which appear to be teleologically favorable. Fung called this experimental process *preconditioning*. Whereas few have sought to understand the underlying mechanisms of preconditioning, most simply exploit it to obtain pseudoelastic responses which are easier to describe mathematically and which appear to be more physiologic in many cases because of the periodic loading experienced by many soft tissues.

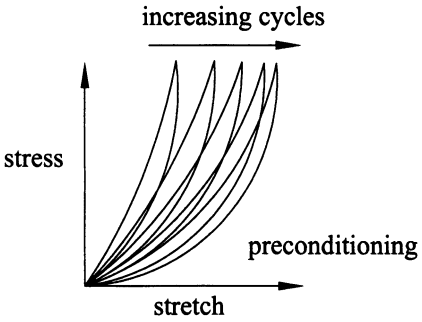

FIGURE 6.4 Preconditioning response exhibited by many soft tissues. Note that the response becomes more extensible and eventually nearly repeatable after a sufficient number of cycles of loading.

Inasmuch as linear elasticity is easily described mathematically, we typically do not think deeply about its implications. Yet, one of the remarkable consequences of a linear stress–strain relation is that it is unique: There is but one way to draw a straight line (i.e., $y = mx + b$). Nonlinear behavior, on the other hand, not only requires the use of a more complex function to fit the stress–strain data, it is also not necessarily unique. Referring to the loading response in Fig. 6.2, for example, one investigator may "see" a parabola and thus suggest a quadratic relationship between stress and stretch, whereas another investigator may see a trigonometric relationship and postulate a tangent function to describe the data. Indeed, because of the inherent scatter in experimental data, multiple functions may be found to describe the data similarly, thus raising the question: What is the best constitutive descriptor for this behavior?

Again, Fung offered a very helpful approach. Fung suggested that instead of plotting stress versus strain (or stretch), we could plot the stiffness as a function of stress. Strictly speaking, *stiffness* is defined as a change in stress with respect to a change in a conjugate strain (or stretch); thus, it is the slope of a stress–strain or stress–stretch curve. To appreciate this, let us consider a simple, 1-D, linearly elastic response. If $\sigma = E\varepsilon$, where E is the Young's modulus, then the stiffness $K = d\sigma/d\varepsilon = E$ for all σ; that is, if we plotted K versus σ, we would obtain a constant value. Integrating then, we would obtain

$$\int \frac{d\sigma}{d\varepsilon} d\varepsilon = \int E\, d\varepsilon \rightarrow \sigma = E\varepsilon + c_0, \tag{6.9}$$

where $c_0 = 0$ if the stress is zero at zero strain, thus yielding the (previously unknown) stress–strain relation. Let us now see what Fung observed.

Fung performed one-dimensional extension tests on excised strips of mesentery, a thin collagenous membrane found in the abdomen. Recalling from Chap. 3 that there are actually multiple definitions of stress (σ is the so-called

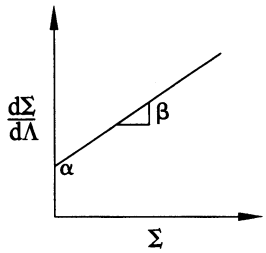

FIGURE 6.5 Fung's idea to plot stiffness (i.e., a change in stress with respect to stretch, $d\Sigma/d\Lambda$ in one dimension) versus the first Piola–Kirchhoff stress (Σ), which, for many tissues, results in a nearly linear relationship.

Cauchy stress, which is a measure of forces acting over current oriented areas, whereas Σ is the so-called nominal or first Piola–Kirchhoff stress, which is a measure of the force acting over an original oriented area), Fung chose to use Σ as his measure of stress and Λ as his measure of extension (Λ being a stretch ratio, which is a component of the deformation gradient as seen in Example 6.1). Doing so, Fung obtained a result similar to that shown in Fig. 6.5: a near-linear relation between the stiffness $d\Sigma/d\Lambda$ and the first Piola–Kirchhoff stress Σ; that is, the data appeared to be well described by

$$\frac{d\Sigma}{d\Lambda} = \alpha + \beta\Sigma, \tag{6.10}$$

which is a first-order, nonhomogenous, linear differential equation with a constant coefficient. This equation is solved easily using either standard methods for differential equations (Appendix 8 of Chap. 8) or a direct integration. For example, for this class of differential equations, we expect a homogenous solution to be of an exponential form and a particular solution to be a constant; that is, let our trial solution be of the form

$$\Sigma = c_1 e^{c_2\Lambda} + c_3. \tag{6.11}$$

To find the values of the unknown constants, note that

$$\frac{d\Sigma}{d\Lambda} = c_1 e^{c_2\Lambda} c_2 = (\Sigma - c_3)c_2 = c_2\Sigma - c_3 c_2 \tag{6.12}$$

whereby from Eq. (6.10), we find that

$$c_2\Sigma - c_3 c_2 = \beta\Sigma + \alpha \rightarrow \begin{cases} c_2 = \beta \\ c_3 = \dfrac{-\alpha}{\beta}. \end{cases} \tag{6.13}$$

To find c_1, we need another condition. For example, if we require the stress Σ to be zero when the strain is zero (i.e., the stretch $\Lambda = 1$), then

$$0 = c_1 e^{\beta} - \frac{\alpha}{\beta} \rightarrow c_1 = \frac{\alpha}{\beta} e^{-\beta} \tag{6.14}$$

and, therefore, the solution to the *experimentally* obtained stress–stretch relation is

$$\Sigma = \frac{\alpha}{\beta} e^{-\beta} e^{\beta\Lambda} - \frac{\alpha}{\beta} \rightarrow \Sigma = \frac{\alpha}{\beta}\left(e^{\beta(\Lambda-1)} - 1\right), \tag{6.15}$$

where α and β are the experimentally measurable intercept and slope, respectively, in Fig. 6.5. Hence, rather that *guessing* functional forms for a stress–stretch relation (e.g., quadratic or trigonometric), Fung used a clever way of replotting the data as stiffness versus stress that revealed a linear relation, which, in turn, unambiguously suggested an exponential form of the constitutive relation. Although plots of stiffness versus stress are not perfectly linear for all tissues over all ranges of stress of interest, years of experience have revealed that exponential constitutive relations often provide good descriptions of the data for certain conditions. See, for example, the fit of a multiaxial exponential relation to data on epicardium in Fig. 6.6.

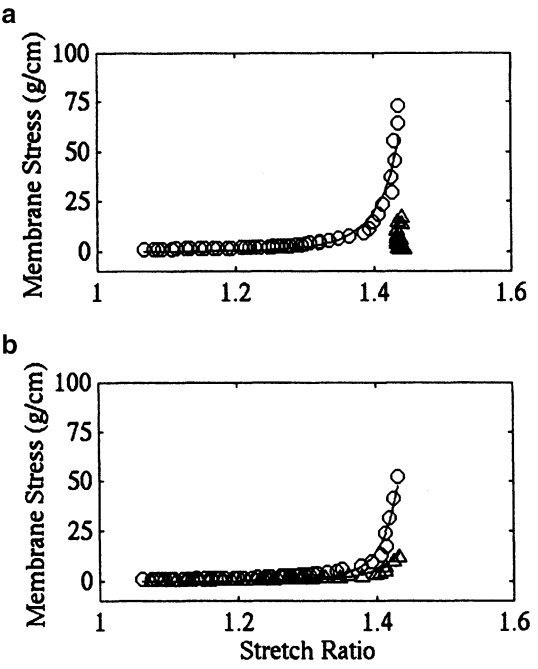

FIGURE 6.6 Fit (solid lines) to biaxial data (open symbols) for excised biaxially stretched epicardium based on a Fung-type exponential relation. [From the author's laboratory (courtesy of J. Harris)].

Given the existence of so many different soft tissues in the body, each having unique structure and function and subjected to different multiaxial stresses and deformations, it should not be surprising that there is a wide variety of proposed constitutive relations in the literature. That is, despite the success of Fung's exponential as well as other functional relations, there is still no general agreement on the "best" relations for any given soft tissue. This situation is in stark contrast to the general acceptance since the mid-1800s of Hooke's law as a descriptor of LEHI behavior (cf. Sect. 2.6.1). There is, therefore, a pressing need for continued research into constitutive relations for soft tissues. For more discussion of this need and comparisons of other successful nonlinear constitutive relations to experimental data, see Humphrey (2002). Here, let us conclude our discussion with two observations.

First, although there is a pressing need for improved, well-accepted nonlinear constitutive functions for many soft tissues, we must remember what a constitutive relation is: It is a mathematical descriptor of particular behaviors exhibited by a material under well-defined conditions, which is to say, it is *not* a descriptor of the material. All materials, including soft tissues, exhibit different behaviors under different conditions; hence, we should expect that multiple constitutive relations will be needed for each tissue depending on the condition of interest. For example, a pseudoelastic relation may be sufficient to describe the cyclic behavior of an artery under physiological conditions, but a viscoelastic descriptor may be needed to describe the artery's response during balloon angioplasty, a thermomechanical relation may be needed to analyze the thermal ablation of an atherosclerotic lesion–artery complex, and a growth and remodeling relation may be needed to describe the long-term response of an artery to hypertensive conditions. Thus, when we say that there is a pressing need for improved, well-accepted relations, this does not suggest that we should seek a single relation that describes well all behaviors under all conditions. Rather, we will still need multiple improved relations for specific conditions of interest. Constitutive formulations, which combine theory and experimentation, thereby remain one of the most important and challenging aspects of biomechanics.

Second, it is important to note that although there are many different measures of stress, they are not independent. It can be shown, for example, that the Cauchy and the first Piola–Kirchhoff stresses are related through the deformation gradient (which, as a fundamental measure of motion, relates undeformed and current areas over which a force must act), namely (Humphrey 2002)

$$[\sigma] = \frac{1}{\det[F]}[F][\Sigma] \leftrightarrow [\Sigma] = \det[F][F]^{-1}[\sigma], \tag{6.16}$$

where $\det[F]$ denotes the determinant and $[F]^{-1}$ denotes the inverse of $[F]$. The latter is defined such that $[F]^{-1}[F] = [I] = [F][F]^{-1}$. Recall that matrix operations are discussed in Appendix 6.

For example, let us consider a simple 1-D stress test wherein a sample is extended in the "1" direction as in the test by Fung on mesentery. It can be shown that the motion is well described by

$$x = \Lambda X, \quad y = \lambda Y, \quad z = \lambda Z \tag{6.17}$$

and, thus, from Eq. (6.4)

$$[F] = \begin{bmatrix} \Lambda & 0 & 0 \\ 0 & \lambda & 0 \\ 0 & 0 & \lambda \end{bmatrix}. \tag{6.18}$$

Now, if the behavior is incompressible or nearly so, as is the case for many tissues, including soft tissues, then volume is conserved and $\det[F] = 1$. Hence $\lambda = 1/\sqrt{\Lambda}$. Show that this is true by computing the undeformed and deformed volumes and setting them equal. If the associated first Piola–Kirchhoff stress is measured as

$$[\Sigma] = \begin{bmatrix} \Sigma_{11} & 0 & 0 \\ 0 & 0 & 0 \\ 0 & 0 & 0 \end{bmatrix} = \begin{bmatrix} \dfrac{f}{A_o} & 0 & 0 \\ 0 & 0 & 0 \\ 0 & 0 & 0 \end{bmatrix}, \tag{6.19}$$

where f is the applied load and A_o is the undeformed area over which the load "acts," then the Cauchy stress is

$$[\sigma] = \frac{1}{1}\begin{bmatrix} \Lambda & 0 & 0 \\ 0 & \dfrac{1}{\sqrt{\Lambda}} & 0 \\ 0 & 0 & \dfrac{1}{\sqrt{\Lambda}} \end{bmatrix}\begin{bmatrix} \dfrac{f}{A_o} & 0 & 0 \\ 0 & 0 & 0 \\ 0 & 0 & 0 \end{bmatrix} = \begin{bmatrix} \Lambda\dfrac{f}{A_o} & 0 & 0 \\ 0 & 0 & 0 \\ 0 & 0 & 0 \end{bmatrix}, \tag{6.20}$$

where $\det[F] \equiv 1$. From Fig. 6.7, we note further that $\Lambda = l/L$ and incompressibility requires that $lA = LA_o$ or $A = A_o/\Lambda$. Hence, we see that the only non-zero component of the Cauchy stress is

$$\sigma_{11} = \frac{\Lambda f}{A_o} = \frac{f}{A_o/\Lambda} = \frac{f}{A}; \tag{6.21}$$

that is, the value of the Cauchy stress is computed as the force acting over the current area A as expected. Perhaps more importantly, however, Eq. (6.16) allows us to compute the Cauchy stress for Fung's mesentery sample in terms of his exponential constitutive relation derived for the first Piola–Kirchhoff stress [Eq. (6.15)]. For the uniaxial test on mesentery, therefore, we have

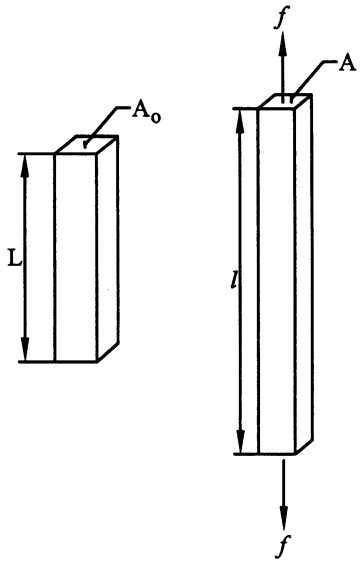

FIGURE 6.7 Uniaxial sample subjected to a uniform axial stress; note the dimensions in the undeformed and deformed configurations.

$$\sigma_{11} = \Lambda\Sigma_{11} = \Lambda\frac{\alpha}{\beta}\left(e^{\beta(\Lambda-1)} - 1\right). \tag{6.22}$$

Whereas the first Piola–Kirchhoff stress is often preferred by experimentalists, for they only have to measure the cross-sectional area A_o (in uniaxial tests) once, in contrast to each A at each f, the Cauchy stress is often preferred in the solution of boundary value problems [cf. Eqs. (3.8)–(3.10)]. Fortunately, relations such as Eq. (6.16) allow us to compute one type of stress from another, thus allowing us to work with that which is more convenient in each case. Indeed, this is a comparable situation to our use of stress transformation equations in Chap. 2, which allow us to determine components relative to the most convenient coordinate system and then to calculate from them the components relative to any coordinate system that is desired. We conclude, therefore, by noting yet another definition of stress, the second Piola–Kirchhoff stress $[S]$ that is often useful in constitutive formulations in nonlinear elasticity. It is related to the Cauchy and (first) Piola–Kirchhoff stress via

$$[\sigma] = \frac{1}{\det[F]}[F][S][F]^T, \quad [\Sigma] = [S][F]^T. \tag{6.23}$$

Albeit related to $[\sigma]$ and $[\Sigma]$, $[S]$ is very different—it does not have a physical interpretation. $[S]$ can be shown to be a measure of a well-defined but fictitious force acting on the actual undeformed area. The utility of $[S]$ lies in its mathematical relationship to the Green strain $[E]$. It can be shown, for example, that $[S]$ can be determined by differentiating a scalar "strain-energy function"

W with respect to $[E]$, which is to say that each component of $[S]$ is found by taking derivatives of W with respect to the associated components of $[E]$, as, for example,

$$S_{11} = \frac{\partial W}{\partial E_{11}}, \quad S_{12} = \frac{\partial W}{\partial E_{12}}, \quad \text{etc.} \tag{6.24}$$

Here, E_{11} represents E_{XX} in Cartesians or even E_{RR} in cylindricals. This situation is comparable to that discussed in Exercise 2.26, in which it was noted that a similar strain-energy W can be thought of as the area under the linear stress–strain curve for a 1-D LEHI behavior, with $\sigma_{xx} = E\varepsilon_{xx}$ and, thus, $W = 1/2(\varepsilon_{xx})\sigma_{xx} = 1/2(E)\varepsilon^2{}_{xx}$, and, finally, $\sigma_{xx} = \partial W/\partial \varepsilon_{xx}$. Equation (6.24) and its related constitutive relations for W are much more general, however, being valid for nonlinear elastic behavior over large strains. For example, motivated by (but not directly derivable from) the 1-D exponential result of Eq. (6.15), Fung (1990) postulated that a potentially useful strain-energy function may be

$$W = \frac{1}{2}c\left(e^Q - 1\right), \tag{6.25}$$

where, for orthotropy,

$$\begin{aligned} Q_{\text{orth}} = {} & c_1E_{11}^2 + c_2E_{22}^2 + c_3E_{33}^2 + 2c_4E_{11}E_{22} + 2c_5E_{22}E_{33} + 2c_6E_{33}E_{11} \\ & + c_7\left(E_{12}^2 + E_{21}^2\right) + c_8\left(E_{23}^2 + E_{32}^2\right) + c_9\left(E_{31}^2 + E_{13}^2\right) \end{aligned} \tag{6.26}$$

and c and c_1–c_9 are material parameters and $E_{11}, \ldots, E_{33}$ are the nine components of $[E]$ relative to a particular coordinate system. Hence, for example,

$$\begin{aligned} S_{11} &= \frac{\partial W}{\partial E_{11}} = \frac{1}{2}ce^Q(2c_1E_{11} + 2c_4E_{22} + 2c_6E_{33}) \\ &= ce^Q(c_1E_{11} + c_4E_{22} + c_6E_{33}) \end{aligned} \tag{6.27}$$

with other components of $[S]$ computed similarly. This relatively simple multiaxial relation has been shown to provide reasonable fits to data for various soft tissues, including myocardium, arteries, and skin (Fung 1990), but, again, there remains a need to search for improved relations in many cases. One advantage of Eqs. (6.25)–(6.26) is that, similar to a generalized Hooke's law (which can be found from a W that is quadratic in the components of $[\varepsilon]$), one can specify simplifications in the constants in Q for different material symmetries [cf. Eqs. (2.69), (2.75), and (2.77)]. Whereas one needs all nine values of c_1–c_9 for orthotropy, this number reduces to five for transverse isotropy and

only two for isotropy. Specifically, for transverse isotropy, with the preferred direction being the (3) direction, $c_1 = c_2$, $c_5 = c_6$, $c_8 = c_9$; thus,

$$\begin{aligned} Q_{\text{trans}} = {} & c_1\left(E_{11}^2 + E_{22}^2\right) + c_3 E_{33}^2 + 2c_4 E_{11}E_{22} + 2c_5(E_{11} + E_{22})E_{33} \\ & + c_7\left(E_{12}^2 + E_{21}^2\right) + c_8\left(E_{23}^2 + E_{32}^2 + E_{13}^2 + E_{31}^2\right), \end{aligned} \tag{6.28}$$

where $c_7 = 2(c_1 - c_4)$. Finally, for isotropy, $c_1 = c_3$, $c_4 = c_5$, $c_7 = c_8$; thus,

$$\begin{aligned} Q_{\text{iso}} = {} & c_1\left(E_{11}^2 + E_{22}^2 + E_{33}^2\right) + 2c_4(E_{11}E_{22} + E_{22}E_{33} + E_{33}E_{11}) \\ & + c_7\left(E_{12}^2 + E_{21}^2 + E_{23}^2 + E_{32}^2 + E_{13}^2 + E_{31}^2\right). \end{aligned} \tag{6.29}$$

Note that for isotropy, we can alternatively write Q as

$$\begin{aligned} Q_{\text{iso}} = {} & \alpha(E_{11} + E_{22} + E_{33})^2 + \beta\left(-E_{12}^2 - E_{21}^2 - E_{23}^2 - E_{32}^2 - E_{13}^2\right. \\ & \left. - E_{31}^2 + E_{11}E_{22} + E_{22}E_{33} + E_{33}E_{11}\right), \end{aligned} \tag{6.30}$$

where $\alpha = c_1$ and $\beta = -c_7$ or, recognizing that these combinations of strains are invariant under coordinate transformations,

$$Q_{\text{iso}} = \alpha I_E^2 + \beta II_E, \tag{6.31}$$

where

$$\begin{aligned} I_E &= E_{11} + E_{22} + E_{33}, \\ II_E &= E_{11}E_{22} + E_{22}E_{33} + E_{33}E_{11} - 2E_{12}E_{21} - 2E_{23}E_{32} - 2E_{31}E_{13}, \end{aligned} \tag{6.32}$$

with $E_{12} = E_{21}$, $E_{13} = E_{31}$, and $E_{23} = E_{32}$ by definition. This form for Q was found to describe the behavior of lung parenchyma reasonably well (Fung 1993). Let us now explore a useful experiment and the utility of Fung's exponential (pseudo)strain-energy function.

6.3 Design of Biaxial Tests on Planar Membranes

6.3.1 Biological Motivation

A membrane is defined differently in biology and mechanics. In biology, a membrane is a thin layer of tissue that covers a surface or separates a space; examples include the cell membrane, the basement membrane in the arterial wall, the pleural membrane which covers the lung, the epicardial membrane which covers the heart, and the mesentery within the abdomen. Consideration of the important structural roles played by these membranes, as well as membranes such as the urinary bladder and saccular aneurysms, reveals the need to

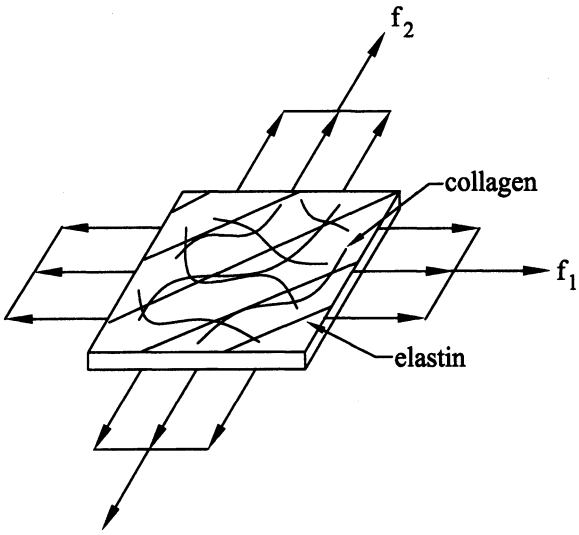

FIGURE 6.8 Schema of the complex distributions of elastin and collagen in a planar tissue such as the epicardium, pericardium, pleura, or mesentery. Such tissues are easily tested in a biaxial setting (i.e., subjected to orthogonal in-plane loads f_1 and f_2).

understand the associated mechanics. In mechanics, a membrane is defined as a structure having two dimensions much greater than the third and, in particular, a structure that offers negligible resistance to bending; that is, the in-plane load-carrying capability is most important in membranes, a simple example being that a soap bubble resists a distension pressure solely through its (in-plane) surface tension. Experience has revealed that most biological membranes behave mechanically as membranes within the context of mechanics. Hence, in many cases, we are interested primarily in their in-plane properties.

Many biological membranes consist primarily of a 2-D plexus of elastin and collagen embedded in a viscous ground substance matrix consisting of proteoglycans and water. Moreover, in most cases, the elastin and collagen fibers have complex orientations (Fig. 6.8) that give rise to anisotropic responses. For this reason, it is not sufficient to study the material behavior using a single uniaxial test. Rather, it is useful to employ in-plane biaxial stretching tests to assess the mechanical behavior. Question: Why would bending tests such as those in Chap. 5 not be useful?

6.3.2 Theoretical Framework

In most cases, biaxial tests are designed such that multiple, individual loading fixtures are applied to each of the four sides of the sample (Fig. 6.9). The primary reason for this is that stretching in one direction will induce an associated shortening (i.e., Poisson-like effect) in the orthogonal direction. Whereas single clamps on each side would impede such deformations, individual loading fixtures do not, hence their use. Note, however, that individual

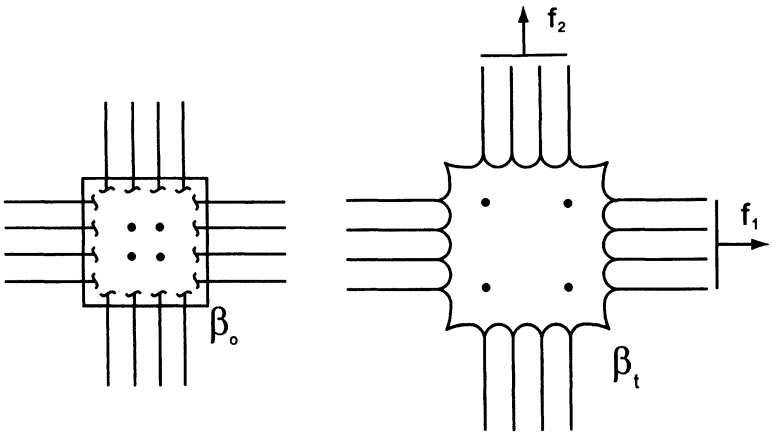

FIGURE 6.9 Specimen prepared for biaxial testing, loaded via multiple individual loading strings per side. Individual loading fixtures allow the tissue to thin in one direction when pulled in the orthogonal direction, which is important, yet they also introduce stress concentrations at the loading sites. From Humphrey (2002), with permission.

(point) loads introduce *stress concentrations* at the points of application, where the tissue is likely to fail first if overloaded. Thus, if the experiment is designed to investigate failure properties, one often introduces a circular or elliptical hole in the center of the specimen to control and initiate the failure process. We will not consider such tests here, but they have applicability to the design of incisions and wound healing, including cataract surgery and the removal of the lens, as well as to the study of failure mechanisms. Rather, let us consider subfailure tests wherein one focuses on the central region in which the deformation is measured (similar to the use of a gauge length in the axially loaded rod experiment). Because of the large deformations, however, we cannot use strain gauges as in tests on bone. Question: How then should we measure the deformation? Recalling our relation for the deformation gradient [Eq. (6.4)], note that we simply need to know the current positions (x, y) of points that were originally at (X, Y) in an undeformed reference configuration. One way to accomplish this is to *track* markers that are placed in the central region of the sample. In general, we place multiple markers (e.g., 3, 4, 9,...) and use so-called *interpolation functions* to obtain continuous expressions for

$$x = f(X, Y) \quad \text{and} \quad y = g(X, Y) \tag{6.33}$$

or, similarly, for the displacements,

$$u_x = x - X = f(X, Y) - X \quad \text{and} \quad u_y = y - Y = g(X, Y) - Y, \tag{6.34}$$

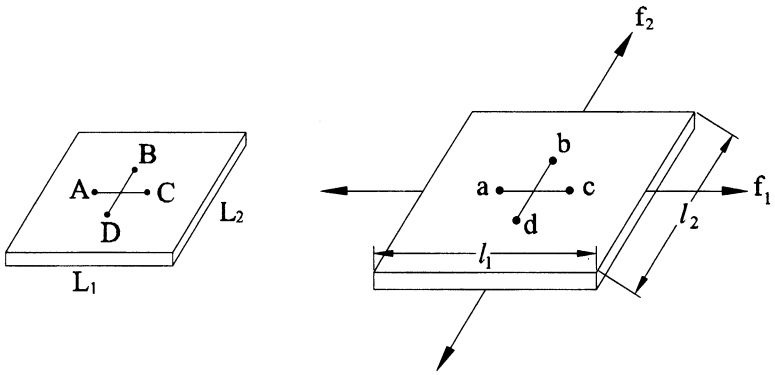

FIGURE 6.10 Dimensions of a biaxial specimen in the central region, before and after loading and assuming a homogeneous deformation; a, b, c, and d denote tracking markers for computing strain in the central region of the soft tissue sample. Strain gauges cannot be used, of course, because of their extreme stiffness.

so that we can compute the requisite deformation or displacement gradients. For such approaches, see Humphrey (2002). Here, we will simply assume that the deformation is homogeneous (i.e., uniform) in the central region, thus allowing us to compute pointwise quantities like strain over finite lengths. In particular, referring to Fig. 6.10 (let $\ell_1 = \ell_x$ and $\ell_2 = \ell_y$), let

$$\overline{ac} = l_x, \quad \overline{bd} = l_y \tag{6.35}$$

and, similarly, in the undeformed configuration

$$\overline{AC} = L_x, \quad \overline{BD} = L_y \tag{6.36}$$

such that [cf. Eq. (2.50)]

$$x = \Lambda_1 X = \frac{l_x}{L_x} X, \quad y = \Lambda_2 Y = \frac{l_y}{L_y} Y. \tag{6.37}$$

Although a membrane is treated two dimensionally, there will be thinning in the third direction. If we account for this via the stretch $\Lambda_3 = h/H$, where h and H are the deformed and undeformed thickness, respectively, we have

$$z = \Lambda_3 Z = \frac{h}{H} Z. \tag{6.38}$$

Hence, for this simple in-plane biaxial test, we have, from Eq. (6.4),

$$[F] = \begin{bmatrix} \frac{\partial x}{\partial X} & \frac{\partial x}{\partial Y} & \frac{\partial x}{\partial Z} \\ \frac{\partial y}{\partial X} & \frac{\partial y}{\partial Y} & \frac{\partial y}{\partial Z} \\ \frac{\partial z}{\partial X} & \frac{\partial z}{\partial Y} & \frac{\partial z}{\partial Z} \end{bmatrix} = \begin{bmatrix} \Lambda_1 & 0 & 0 \\ 0 & \Lambda_2 & 0 \\ 0 & 0 & \Lambda_3 \end{bmatrix}, \tag{6.39}$$

where $\Lambda_1 = l_x/L_x$, $\Lambda_2 = l_y/L_y$, and $\Lambda_3 = h/H$ are all measurable in principle, although on-line measurement of changes in thickness are problematic in many cases. It is for this reason that experimentalists often invoke the incompressibility constraint ($\det [F] = 1$), for this allows the thinning to be inferred from the more easily measured in-plane quantities. Indeed, because many tissues are nearly incompressible under many cases of cyclic loading, volume conservation yields

$$l_x l_y h = L_x L_y H \rightarrow \Lambda_1 \Lambda_2 \Lambda_3 = 1, \tag{6.40}$$

where we recognize that $\Lambda_1 \Lambda_2 \Lambda_3 = \det[F]$.

Now, for the constitutive behavior. Recall from Chaps. 1 and 2 that a general formulation requires five general steps: DEICE, which is to say, *delineating* general characteristic behaviors, *establishing* an appropriate theoretical framework, *identifying* a specific functional relationship between the independent and dependent constitutive parameters, *calculating* best-fit values of the associated material parameters, and *evaluating* the predictive capability of the final relation. In the present context, we assume that general characteristics are a preconditionable nonlinear, pseudoelastic, homogeneous, anisotropic, incompressible behavior of a membrane having negligible bending stiffness and subject to large in-plane deformations. One possible theoretical framework is thus the theory of large-deformation membrane elasticity, which we will employ.

In practice, identifying the specific functional form of the constitutive relation, for conditions of interest, is the most challenging of the five steps. In general, there are three ways by which this can be accomplished: via an educated guess that is based on extant observations, theoretical restrictions, and prior experience; via a formal theoretical derivation, often based on statistical mechanical arguments; or via inference directly from clever interpretations of experimental data. Fung's identification of the 1-D exponential $\Sigma = \Sigma(\Lambda)$ relation in Eq. (6.15) is a good example of an experimentally based identification. Such identifications are much more difficult in two or three dimensions however, and the interested reader is referred to Humphrey (2002) for details. Here, let us proceed by assuming (guessing) a 2-D Fung-type exponential relation of the form

$$W = c\left(e^{Q} - 1\right), \quad Q = c_1 E_{11}^2 + c_2 E_{22}^2 + 2c_3 E_{11} E_{22}, \tag{6.41}$$

similar to the 3-D form given in Eqs. (6.25) and (6.26). Note that we ignore shear here because only E_{11} and E_{22} are assumed to be nonzero in our biaxial test. Note, too, that the units of W are energy per volume; we could alternatively use a strain energy w defined per surface area (of the membrane), where $w \sim HW$ and H is the undeformed thickness.

From Eqs. (6.23) and (6.24), therefore, we have for Eqs. (6.39) and (6.41) the following:

$$[\sigma] = \frac{1}{\Lambda_1 \Lambda_2 (h/H)} \begin{bmatrix} \Lambda_1 & 0 & 0 \\ 0 & \Lambda_2 & 0 \\ 0 & 0 & \Lambda_3 \end{bmatrix} \begin{bmatrix} S_{11} & 0 & 0 \\ 0 & S_{22} & 0 \\ 0 & 0 & 0 \end{bmatrix} \begin{bmatrix} \Lambda_1 & 0 & 0 \\ 0 & \Lambda_2 & 0 \\ 0 & 0 & \Lambda_3 \end{bmatrix}, \tag{6.42}$$

where [cf. Eq. (6.27)]

$$S_{11} = \left(2ce^{Q}\right)(c_1 E_{11} + c_3 E_{22}), \quad S_{22} = \left(2ce^{Q}\right)(c_2 E_{22} + c_3 E_{11}) \tag{6.43}$$

and, therefore,

$$\sigma_{11} = \frac{\Lambda_1}{\Lambda_2}\left(\frac{H}{h}\right)\left(2ce^{Q}\right)(c_1 E_{11} + c_3 E_{22}) \tag{6.44}$$

and

$$\sigma_{22} = \frac{\Lambda_2}{\Lambda_1}\left(\frac{H}{h}\right)\left(2ce^{Q}\right)(c_2 E_{22} + c_3 E_{11}), \tag{6.45}$$

with $\sigma_{33} = 0$. Note that this is an example of a state of plane stress, which was defined in Chap. 2. The nonzero in-plane tensions that represent the load-carrying capability of the membrane are thus,

$$T_1 = \sigma_{11} h = \left(\frac{\Lambda_1}{\Lambda_2}\right) Hce^{Q}\left[c_1\left(\Lambda_1^2 - 1\right) + c_3\left(\Lambda_2^2 - 1\right)\right], \tag{6.46}$$

$$T_2 = \sigma_{22} h = \left(\frac{\Lambda_2}{\Lambda_1}\right) Hce^{Q}\left[c_2\left(\Lambda_2^2 - 1\right) + c_3\left(\Lambda_1^2 - 1\right)\right], \tag{6.47}$$

where T_1 and T_2 are the principal tensions (force per length). Moreover, from Eq. (6.16), we know that

$$[\sigma] = \frac{1}{\Lambda_1\Lambda_2(h/H)} \begin{bmatrix} \Lambda_1 & 0 & 0 \\ 0 & \Lambda_2 & 0 \\ 0 & 0 & \Lambda_3 \end{bmatrix} \begin{bmatrix} \dfrac{f_1}{A_{1o}} & 0 & 0 \\ 0 & \dfrac{f_2}{A_{2o}} & 0 \\ 0 & 0 & 0 \end{bmatrix} \tag{6.48}$$

where A_{1o} is the easily measured original area over which the resultant force f_1 acts in the undeformed configuration and similarly for A_{2o}. Hence, we have

$$T_1 = \sigma_{11}h = \frac{H}{\Lambda_2}\left(\frac{f_1}{A_{1o}}\right), \quad T_2 = \sigma_{22}h = \frac{H}{\Lambda_1}\left(\frac{f_2}{A_{2o}}\right), \tag{6.49}$$

which allows us to relate our theoretically predicted and experimentally determined principal *tensions* (sometimes called stress resultants); that is, Eqs. (6.46) and (6.47) combined with Eq. (6.49) allow us to *calculate* the values of the material parameters as demanded in the fourth step of the DEICE procedure. Although we only have four "unknown" material parameters (c, c_1, c_2, and c_3), which may imply the need for only two data points (i.e., two sets of σ_{11} versus Λ_1 and σ_{22} versus Λ_2 data, which provide four equations for our four unknowns), it is common practice to determine the values of the parameters in a least-squares sense to avoid the consequences of the inevitable experimental errors. Because c_1, c_2, and c_3 appear in the exponential, one must use a *nonlinear least-squares* method to determine the best-fit values. In principle, then, we seek to minimize the sum of the squares of the differences between theoretically predicted and experimentally determined tensions at $j = 1, 2, \ldots n$ equilibrium configurations by minimizing the objective function e:

$$\begin{aligned} e = \sum_{j=1}^{n} \Bigg\{ & \left[\left(\frac{\Lambda_1}{\Lambda_2}\right) cHe^{Q}\left[c_1\left(\Lambda_1^2 - 1\right) + c_3\left(\Lambda_2^2 - 1\right)\right] - \frac{H}{\Lambda_2}\left(\frac{f_1}{A_{1o}}\right) \right]_j^2 \\ & + \left[\left(\frac{\Lambda_2}{\Lambda_1}\right) cHe^{Q}\left[c_2\left(\Lambda_2^2 - 1\right) + c_3\left(\Lambda_1^2 - 1\right)\right] - \frac{H}{\Lambda_1}\left(\frac{f_2}{A_{2o}}\right) \right]_j^2 \Bigg\} \end{aligned} \tag{6.50}$$

where we note that the effect of thickness H can be removed entirely as a common factor as expected of this 2-D analysis. Minimization of e is accomplished, of course, by solving the simultaneous nonlinear equations given by

$$\frac{\partial e}{\partial c} = 0, \quad \frac{\partial e}{\partial c_1} = 0, \quad \frac{\partial e}{\partial c_2} = 0, \quad \frac{\partial e}{\partial c_3} = 0. \tag{6.51}$$

Commercially available codes accomplish this easily, provided the functional form of the constitutive equation is well chosen; thus, we need not be concerned with numerical details here. Of course, once the best-fit values of the parameters

are calculated, one should complete the DEICE procedure by *evaluating* the general predictive capability of the final relation. This is generally accomplished by comparing its predictions to data that were not used in the constitutive formulation. Such validations are essential for engendering confidence in the use of relations determined from relatively simple experiments. Simple experiments are sought by experimentalists, of course, for they ease performance and interpretation, but we must ensure that the associated results hold for the generally much more complex in vivo situations of interest. For example, if we determine a Young's modulus E for cortical bone via a 1-D tension test, we must verify that this value can be used in an analysis of bending wherein the moment-curvature equation (5.22) governs the response. Such issues are even more important in nonlinear relations.

6.4 Stability of Elastomeric Balloons

6.4.1 Biological Motivation

In 1963, C. Dotter forced a catheter retrograde through an occluded iliac artery in a patient to obtain a routine aortogram. In so doing, flow was improved through the previously occluded vessel; this marked the inadvertent beginning of the use of catheters as interventional rather than just diagnostic devices. Indeed, since that time, millions of balloon angioplasties have been performed to open atherosclerotic vessels, and based on the associated successes, other balloon-based procedures have arisen.

For example, Zubkov et al. (1984) were the first to report the use of a balloon dilatation to treat vasospasm in the cerebral vasculature. Simply put, a *vasospasm* is a persistent, nonphysiologic constriction of an artery that reduces distal flow and may thereby lead to ischemia or necrosis. Intracranial vasospasms occur in 30–70 % of all patients who experience a subarachnoid hemorrhage, the most common cause of which is the rupture of an intracranial aneurysm. Although responsible for significant mortality and morbidity, with symptoms typically presenting 3–15 days after the bleed, vasospasm remains poorly understood. Nevertheless, because the reduced lumen associated with vasospasm compromises blood flow, Zubkov et al. suggested that a balloon dilatation could restore the lumen to near its normal value; that is, they reasoned that a controlled injury to the arterial wall could weaken it so that the normal blood pressure could distend the vessel more. Because the affected cerebral vessels are not stiffened by atherosclerosis or supported by significant perivascular tissue, early neuroangioplasty balloons were constructed of latex or silicone in contrast to the much stiffer polyethylene balloons used in traditional coronary or peripheral vessel angioplasty (Fig. 6.11). Experience revealed, however, that the dilatations by the "softer" balloons were difficult to control. In hindsight,

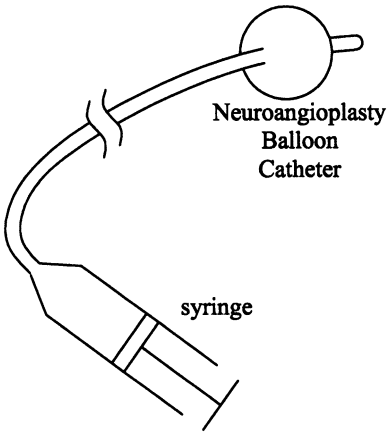

FIGURE 6.11 Schema of a neuroangioplasty balloon, which is constructed out of silicone rather than a polyethylene as in coronary angioplasty balloons.

there are at least two reasons for this, which the design engineer should have anticipated had he or she been familiar with nonlinear elasticity. First, latex rubber exhibits a preconditioning-like (cf. Fig. 6.4) softening effect referred to as the *Mullin's effect*. Hence, the pressure–volume behavior of a given balloon may change from cycle to cycle, thus complicating its control (Fig. 6.12). Many neurointerventionalists would inflate and deflate a balloon before a procedure to ensure that the device did not leak, but this was not a well-specified, repeatable part of the procedure. Second, as we know from common experience, rubber party balloons can exhibit an instability that leads to a rapid expansion at a constant pressure, which again would complicate one's attempt to control the dilatation. Such an instability is similar to that experienced by columns whereby the structure changes shape dramatically due to a small change in load. Hence, let us briefly look at this type of a material/structural instability here.

6.4.2 *Theoretical Framework*

Although we will illustrate the phenomenon of an inflation instability in an elastomeric balloon by considering the simple case of a spherical geometry, let us first consider the more general case of an axisymmetric inflation of a membrane. Axisymmetry implies that the undeformed and deformed shapes of the membrane can each be described by generator curves that define the entire surface when rotated through 2π radians (Fig. 6.13). It can be shown (Humphrey 2002) that the two governing equilibrium equations for an axisymmetric membrane are

$$\frac{d}{dr}(rT_1) = T_2, \quad \kappa_1 T_1 + \kappa_2 T_2 = P, \tag{6.52}$$

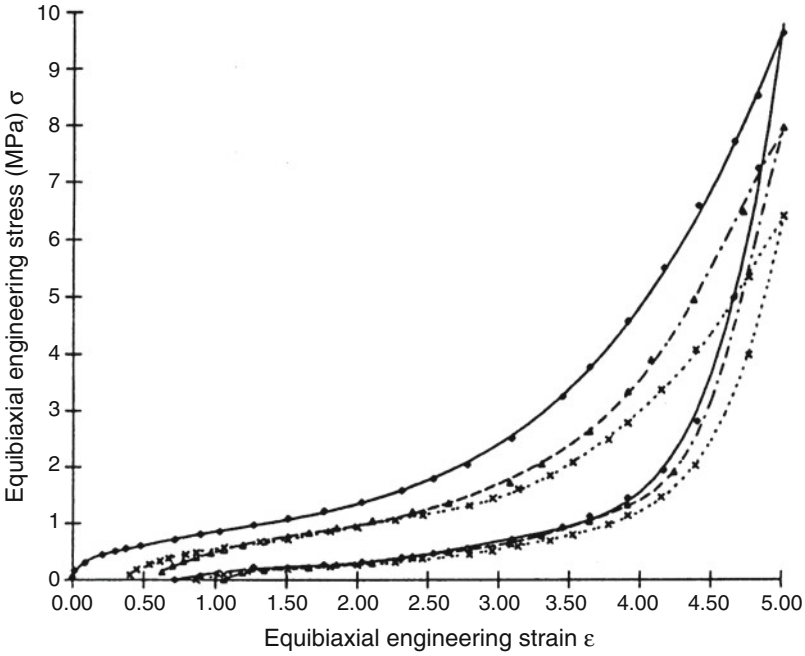

FIGURE 6.12 Pressure–volume behavior of a rubber balloon over a number of inflation/deflation cycles. Note that, like preconditioning of a soft tissue (cf. Fig. 6.4), the balloon stress-softens with repeated loading, an effect called the Mullin's effect. (From Johnson and Beatty (1995), with permission from Elsevier).

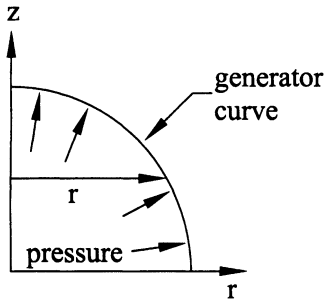

FIGURE 6.13 Pressure–volume geometry for an axisymmetrically inflated membrane. By axisymmetric, we mean that a generator curve can be revolved about an axis to yield the surface of the membrane. Axisymmetry imposes certain restrictions on the material properties and applied loads.

where T_1 and T_2 are the principal tensions (Cauchy stress resultants) in the meridional and circumferential directions, κ_1 and κ_2 are the principal curvatures in the deformed configuration, and $P > 0$ is the transmural (distension) pressure.

The second of these relations is known as Laplace's equation, which is widely used (sometimes misused) in medicine and surgery. Moreover, it can be shown from differential geometry that

$$\frac{d}{dr}(r\kappa_2) = \kappa_1. \tag{6.53}$$

Our goal then is to solve for the tensions T_1 and T_2 in terms of the applied load and measures of the (deformed) geometry [cf. Eq. (3.59)]. Given two equilibrium equations in terms of our two unknown tensions, note that it is often easiest to reduce one of the equations to contain only one of the unknowns. Toward this end, let us substitute for T_2 and κ_1 from Eqs. (6.52) and (6.53), in Laplace's equation such that

$$\kappa_1 T_1 + \kappa_2 T_2 = P \rightarrow \frac{d}{dr}(r\kappa_2)T_1 + \kappa_2 \frac{d}{dr}(rT_1) = P. \tag{6.54}$$

Additionally, note that (check it) this equation can be rewritten as

$$\frac{1}{r}\frac{d}{dr}(r\kappa_2 rT_1) = P, \tag{6.55}$$

which, in turn, can be integrated as (see Appendix 8 of Chap. 8)

$$\int \frac{d}{dr}(r\kappa_2 rT_1)dr = \int Prdr. \tag{6.56}$$

If P is assumed to be constant at each equilibrium state, we thus obtain

$$r^2\kappa_2 T_1 = P\frac{r^2}{2} + c_1 \rightarrow T_1 = \frac{P}{2\kappa_2} + \frac{c_1}{r^2\kappa_2}, \tag{6.57}$$

which must be valid for all r, including $r = 0$; this requirement implies that $c_1 = 0$, which gives us our result for T_1 in terms of the applied load and measure of the geometry, namely P and κ_2. Substituting back into Laplace's equation, we then find the desired relation for T_2 as well. The final results are:

$$T_1 = \frac{P}{2\kappa_2}, \quad T_2 = \frac{P}{\kappa_2}\left(1 - \frac{\kappa_1}{2\kappa_2}\right). \tag{6.58}$$

In Humphrey (2002), it is shown that these equations are fundamental to designing and interpreting inflation tests on axisymmetric membranes as well as to analyzing the stresses in such membranes, such as intracranial saccular aneurysms (cf. Fig. 3.18). Here, however, let us consider but one special case—the inflation of a spherical membrane.

6.4.3 *Inflation of a Neuroangioplasty Balloon*

The two principal curvatures in an inflated spherical membrane (i.e., spherical in its undeformed and deformed configurations) are equal and simply given by 1 over the radius of curvature, which in this special case equals the radius of the deformed sphere a. Hence,

$$\kappa_1 = \kappa_2 = \frac{1}{a} \tag{6.59}$$

and, therefore,

$$T_1 = \frac{Pa}{2} \quad \text{and} \quad T_2 = Pa\left(1 - \frac{a}{2a}\right) = \frac{Pa}{2} \tag{6.60}$$

whereby we see that the tension is uniform and equibiaxial (i.e., $T_1 = T_2$ independent of location r, θ, ϕ) in the sphere (which must be isotropic in-plane for a sphere to inflate into a sphere) and given by

$$T = \frac{Pa}{2}. \tag{6.61}$$

To compute the Cauchy stress from this tension (i.e., Cauchy stress resultant T has units of force per length), we simply divide by the deformed thickness h to obtain

$$\sigma = \frac{T}{h} = \frac{Pa}{2h}, \tag{6.62}$$

which we recognize to be the same result as that obtained in Chap. 3 for the inflation of a thin-walled sphere [Eq. (3.58)], as it should.

One important observation from this derivation, however, is that a is, strictly speaking, not the deformed radius; rather it is the deformed radius of curvature, *curvature* being the controlling geometric feature of axisymmetric membranes [cf. Eq. (6.58)]. Indeed, this simple realization may explain, in part, a long-standing controversy in neurosurgery. If $\sigma \cong Pa/2h$ in a saccular aneurysm and if the mean blood pressure (~110 mmHg) and wall thickness (~100 μm) are similar from patient to patient, one would expect that the larger-diameter lesions would be much more susceptible to rupture. Although larger lesions are often more lethal, many smaller lesions rupture, whereas many larger lesions do not. It is suggested in Humphrey (2002) that this enigma may be due, in part, to the focusing on size rather than shape; that is, a "large" lesion can have a small radius of curvature, whereas a "small" lesion may have a large radius of curvature, curvature being the controlling factor (Fig. 6.14).

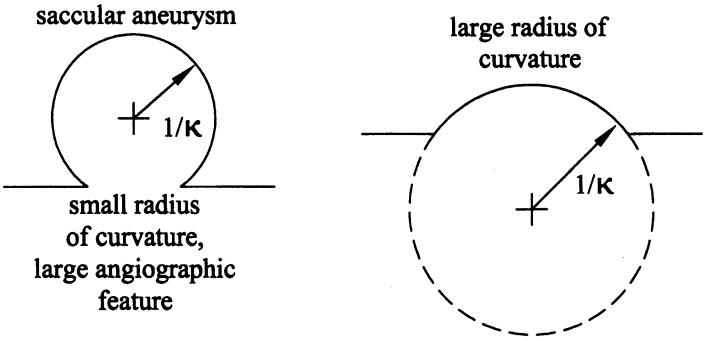

FIGURE 6.14 Radius of curvature for two aneurysms revealing that a larger lesion may have a smaller radius of curvature. Contrary to popular clinical belief, it is curvature, not size, that likely controls the associated biomechanics.

Again, therefore, we are well advised to remember how our governing equations are derived so that we can interpret their implications.

That said, let us return to the problem at hand—the possible instability of a neuroangioplasty balloon, which we idealize as a sphere. It can be shown that the "simplest" descriptor of the behavior of a rubberlike material over moderate stretches (up to ~1.3–1.4) is the so-called neo-Hookean relation. For a membrane, it can be written as (Humphrey 2002)

$$W = C\left(2E_{11} + 2E_{22} + \frac{1}{1 + 2E_{11} + 2E_{22} + 4E_{11}E_{22}} - 1\right), \tag{6.63}$$

where C is a material parameter having units of stress and E_{11} and E_{22} are the principal components of the Green strain [cf. Eq. (6.41) for the Fung material]. Now, for the inflation of a thin-walled sphere, the deformation gradient can be written as

$$[F] = \begin{bmatrix} \Lambda_1 & 0 & 0 \\ 0 & \Lambda_2 & 0 \\ 0 & 0 & \Lambda_3 \end{bmatrix}, \tag{6.64}$$

where $\Lambda_1 = 2\pi a/2\pi A = \Lambda_2$ are the principal stretches in the meridional and circumferential directions, with a and A the deformed and undeformed radii, respectively, and $\Lambda_3 = h/H$ is the principal stretch in the thickness direction, with h and H the deformed and undeformed thicknesses, respectively. Hence, let $\Lambda_1 = \Lambda_2 = a/A = \Lambda$ for convenience. From Eqs. (6.23) and (6.24), therefore, we have

$$[\sigma] = \frac{1}{\det[F]}[F]\left[\frac{\partial W}{\partial E}\right][F]^T, \tag{6.65}$$

where, for the neo-Hookean material behavior,

$$\frac{\partial W}{\partial E_{11}} = C\left(2 + 0 + \frac{(1 + 2E_{11} + 2E_{22} + 4E_{11}E_{22})(0) - 1(2 + 4E_{22})}{(1 + 2E_{11} + 2E_{22} + 4E_{11}E_{22})^2}\right). \tag{6.66}$$

For the $[F]$ given here, Eq. (6.7) reveals that

$$E_{11} = \frac{1}{2}(\Lambda_1^2 - 1) = \frac{1}{2}(\Lambda^2 - 1) \tag{6.67}$$

and similarly for E_{22}. Hence, for the spherical deformation,

$$\begin{aligned}\frac{\partial W}{\partial E_{11}}\Big|_{E_{11}=E_{22}=\frac{1}{2}(\Lambda^2-1)} &= C\left(2 - \frac{2 + 4\left(\frac{1}{2}\right)(\Lambda^2 - 1)}{\left[1 + 4\left(\frac{1}{2}\right)(\Lambda^2 - 1) + 4\left(\frac{1}{4}\right)(\Lambda^2 - 1)^2\right]^2}\right) \\ &= 2C\left(1 - \frac{1 + \Lambda^2 - 1}{\left(1 + 2\Lambda^2 - 2 + \Lambda^4 - 2\Lambda^2 + 1\right)^2}\right)\end{aligned} \tag{6.68}$$

or

$$\frac{\partial W}{\partial E_{11}}\Big|_{E_{11}=E_{22}=\frac{1}{2}(\Lambda^2-1)} = 2C\left(1 - \frac{\Lambda^2}{\Lambda^8}\right) = 2C\left(1 - \frac{1}{\Lambda^6}\right) \tag{6.69}$$

and similarly for $\partial W/\partial E_{22}$. Hence,

$$[\sigma] = \frac{1}{\Lambda^2(h/H)}\begin{bmatrix}\Lambda & 0 & 0\\ 0 & \Lambda & 0\\ 0 & 0 & \frac{h}{H}\end{bmatrix}\begin{bmatrix}2C\left(1 - \frac{1}{\Lambda^6}\right) & 0 & 0\\ 0 & 2C\left(1 - \frac{1}{\Lambda^6}\right) & 0\\ 0 & 0 & 0\end{bmatrix}\begin{bmatrix}\Lambda & 0 & 0\\ 0 & \Lambda & 0\\ 0 & 0 & \frac{h}{H}\end{bmatrix} \tag{6.70}$$

from which we see that

$$\sigma_{11} = \frac{2CH}{h}\left(1 - \frac{1}{\Lambda^6}\right) = \sigma_{22} \tag{6.71}$$

and $\sigma_{33} = 0$, or in terms of the principal tensions, the nonzero values are

$$T_1 = h\sigma_{11} = 2CH\left(1 - \frac{1}{\Lambda^6}\right) = T_2 \equiv T. \tag{6.72}$$

Finally, appealing to equilibrium, Eq. (6.60), we have

$$T = \frac{Pa}{2} \rightarrow P = \frac{2T}{a} = \frac{2}{\Lambda A}\left[2CH\left(1 - \frac{1}{\Lambda^6}\right)\right], \tag{6.73}$$

with $a = \Lambda A$, or

$$P(\Lambda) = \frac{4CH}{A}\left(\frac{1}{\Lambda} - \frac{1}{\Lambda^7}\right). \tag{6.74}$$

Plotting the distension pressure as a function of stretch Λ (i.e., increase in normalized radius a/A) reveals a local maximum [i.e., a transition from a stable loading path to an unstable path, the latter being characterized by a rapid increase in size even in the presence of a diminishing pressure (Fig. 6.15)]. Question: At what values of Λ does this instability occur? To answer this, recall from calculus that we find local extrema by taking the first derivative, namely

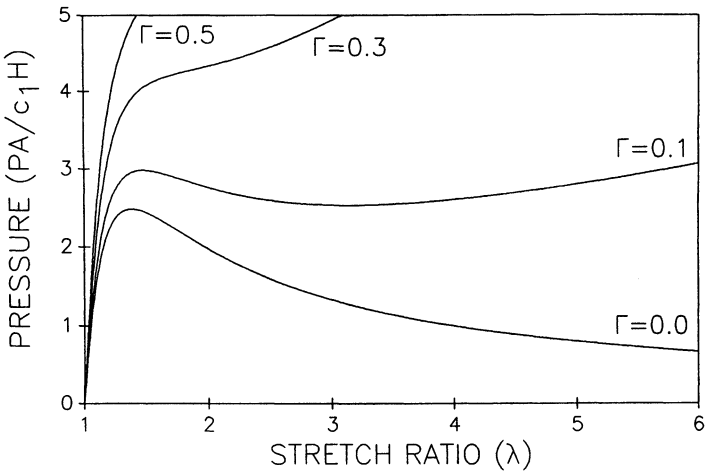

FIGURE 6.15 Pressure–stretch response of spherical rubber (party) balloons with a local maximum revealing a limit point instability (i.e., a transition from a stable to an unstable loading path). Such instabilities depend on the value of one of the material parameters, Γ, that describes the properties of a Mooney-Rivlin rubber; $\Gamma = 0$ for the neo-Hookean case (with $c_1 = C$ here). From Humphrey (2002), with permission.

$$\frac{dP}{d\Lambda} = 0 = \frac{4CH}{A}\left(-\frac{1}{\Lambda^2} + \frac{7}{\Lambda^8}\right) \rightarrow \Lambda^6 = 7. \tag{6.75}$$

Hence, if a near-spherical neuroangioplasty balloon exhibits a neo-Hookean behavior, it is expected to become unstable when $\Lambda = 7^{1/6} \approx 1.38309\ldots$, where $\Lambda = a/A$. This phenomenon explains, in part, why neuroradiologists had trouble controlling the expansion of the neuroangioplasty balloon based on pressure[2] and reveals yet again *the importance of a careful analysis in the design and use of a medical device*. Whereas the present analysis holds approximately for the inflation of an isolated balloon, its inflation within a vessel will change its geometry and thus complicate the analysis. With an appropriate theoretical framework and a reasonable descriptor of the material properties, however, the more complex analysis for nonspherical geometries can be conducted with the aid of a computer. The take-home message here is simply that we must often appreciate and employ the general methods of nonlinear continuum mechanics in the design of many medical devices and, furthermore, in troubleshooting clinical complications.

Observation 6.2. The eye is a remarkable organ; it collects and focuses incoming light on the retina, which, in turn, serves to convert the light into electrical signals that the brain can interpret in bold and vibrant hues of the rainbow. The eye consists of an outer shell, five-sixths of which is the collagenous, opaque sclera and the remainder is the collagenous, transparent cornea. Contained within the eye is the lens, which helps to focus the light on the retina and divides the interior into two chambers: The anterior chamber contains the aqueous humor and the posterior chamber contains the vitreous humor. The iris serves as an aperture for the lens to control the amount of incoming light. The lens is held in place by a thin membrane, the lens capsule, which consists primarily of type IV collagen and allows the curvature of the lens to be changed via contraction and relaxation of the ciliary process. Finally, the posteriorly located optic nerve conducts the signals from the eye to the brain. See Fig. 6.16.

Mechanics plays many roles in ophthalmology. Glaucoma is a disease characterized by an increase in intraocular pressure; it causes pathological changes in the optical disk and concomitant defects in the field of vision. Diagnosis and treatment of this pressure-induced disease requires an understanding of the mechanics. A cataract is a disease of the lens characterized by an opacification that blurs vision and, in extreme cases, causes blindness. Surgical correction involves the removal and replacement of the lens with an intraocular device. Performed over 1.2 million times a year, cataract surgery is currently the most

[2] Whereas pressure is not useful for feedback control, volume is. We revisit this problem in Sect. 10.3 of Chap. 10 in terms of a saline infused balloon.

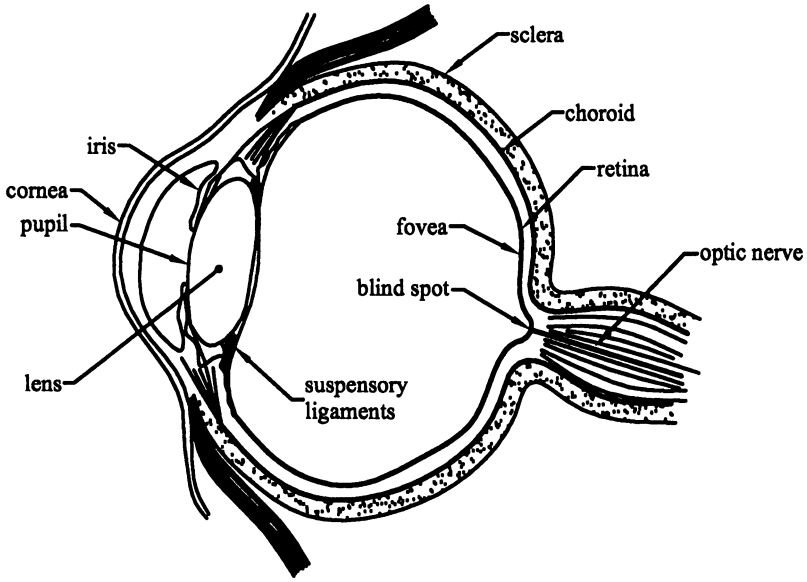

FIGURE 6.16 Schema of the eye. Note, in particular, that the sclera, cornea, and lens capsule have each been assumed to have negligible bending stiffness (i.e., to behave mechanically as membranes) in various biomechanical analyses. One must be cautious, however, in adopting assumptions from the literature. The cornea, for example, has significant bending stiffness, which is likely fundamental to any analysis of clinical procedures such as radial keratotomy or the more popular LASIK surgery. The lens capsule, on the other hand, has much less bending stiffness and may be well described as a membrane in some applications. We are reminded, therefore, that constitutive relations describe the behavior of a material under specified conditions, not the material itself. We must always be mindful of the specific application, particularly in biomechanics.

commonly performed surgery in the United States. The cornea is nearly 18 mm in diameter, less than 1 mm thick in the middle, and has radii of curvature of ~7.8 mm and 6.8 mm at its outer and inner surfaces, respectively. The lens power of the eye is achieved primarily by the curvature of the cornea and secondarily by the lens. In recent years, surgical alteration of the curvature of the cornea has become a popular alternative to the use of eyeglasses or contact lens. This is accomplished by introducing a series of incisions to relieve some of the corneal stress (e.g., radial keratotomy) or by locally shrinking portions of the cornea via thermal denaturation (laser thermokeratoplasty) of the type I collagen in the cornea; in either case, the net effect is that the tension in the pressurized cornea is altered and it thereby changes its curvature and thus refractive power. A rigorous biomechanical analysis of this procedure, for purposes of surgical planning, is beyond the scope of an introductory textbook because of the nonlinear material behavior of the cornea, the need

for fracture-mechanics-type analyses to model the incisions, and the complex geometry. Of course, not only do we need to predict the change in the configuration of the cornea (e.g., thickness and curvature) immediately after the surgery, we must account for changes due to healing and adaptation, the latter of which will be stimulated by changes in the stress field experienced by the cells within the cornea. The interested reader is thus encouraged to research the different applications of mechanics in opthalmology.

Here, however, let us briefly consider the lens capsule. This tissue consists primarily of type IV collagen; it is very thin (~10–20 μm for the anterior lens capsule and 3–4 μm for the posterior lens capsule in the human) and contains a monolayer of epithelial cells on its anterior portion. Clearly, the stress field within the lens capsule is altered due to the surgical removal of the lens and replacement with an intraocular device, which tends to be much smaller than the native lens. One complication of cataract surgery is a secondary opacification of the posterior lens capsule, which often requires a revision, corrective procedure (e.g., thermal ablation). It is thought that this "secondary cataract" is due, in part, to the migration of epithelial cells to the central region of the posterior lens capsule and their production of excessive matrix material. Moreover, it is thought that this altered migration and synthetic activity results from the surgical perturbation of the stress or strain field in the native lens capsule. In other words, mechanotransduction mechanisms likely alter the gene expression by the epithelial cells. It is important, therefore, to quantify the native stress and strain fields in the lens capsule and how they are altered by cataract surgery. Indeed, one would hope that biomechanical analyses could identify designs for the intraocular devices that do not adversely perturb the mechanical environment of the epithelial cells. As a first approximation, one could think of the lens capsule as two hemiellipsoids that are loaded by a transmural pressure (difference in radial stress boundary conditions due to the lens on the inner surface of the lens capsule and the pressure in the aqueous or vitreous humor). Notwithstanding the tractions due to the ciliary process, Eqs. (6.52) and (6.53) could thus be used, to a first approximation, to estimate the membrane stresses in the native configuration. Hence, we see another application of the equations of membrane mechanics.

6.5 Residual Stress and Arteries

6.5.1 Biological Motivation

Hypertension, atherosclerosis, aneurysms, and stroke—these and other vascular diseases continue to be leading causes of mortality and morbidity. Although manifested differently in each case, the fundamental mechanisms by which these diseases begin and then progress relate to basic cellular functions: cell

migration, replication, and apoptosis; the production of vasoactive, growth regulatory, inflammatory and degratory molecules; and the synthesis and organization of constituents of the extracellular matrix. As noted in Chap. 1, many of these cellular functions are influenced, via mechanotransduction mechanisms, by changes in the local mechanical environment. For example, an increased blood pressure nonuniformly increases intramural wall stress, which, in turn, increases cell proliferation and synthesis of the matrix in hypertension, first in the inner portion of the wall but eventually throughout the wall. Conversely, decreased blood flow may lead to decreases in wall shear stress, which, in turn, promote the production of adhesion molecules by the endothelium and the attendant adhesion of monocytes to the endothelium; these monocytes subsequently migrate into the subintimal space, transform into macrophages, and contribute to atherogenesis. There is a need, therefore, to understand arterial mechanics both in health and disease. Whereas a more detailed discussion can be found in Humphrey (2002), here we consider the first step, a simple analysis of wall stress in blood vessels.

First, however, let us briefly review some aspects of the structure of arteries. Despite the wide variety of arteries in the body—from the aorta to the renal arteries, coronary arteries, cerebral arteries, and so on—each of these vessels similarly consist of 3 concentric layers: the tunica intima, tunica media, and tunica adventitia (Fig. 6.17). Indeed, all blood vessels have an intima, which consists of a monolayer of endothelial cells and an underlying basal lamina composed primarily of mesh-like type IV collagen and the adhesion molecules fibronectin and laminin. In addition to being a smooth, nonthrombogenic interface between the blood and the contents of the vascular wall, the endothelium is biologically active. In response to chemical and mechanical stimuli, endothelial cells produce various vasoactive molecules (which dilate or constrict the vessel), growth factors (which promote cell replication or the synthesis of proteins), and factors that regulate the clotting process (e.g., heparan sulfate and the vascular cell adhesion molecule, VCAM-1). Moreover, the endothelium can modify blood-borne substances (e.g., lipids) for transport into the wall, which thereby play an important role in atherosclerosis. In contrast, the medial layer consists primarily of smooth muscle cells embedded in a plexus of elastin, various types of collagen (including types I, III, and V), and proteoglycans. In general, the closer these vessels are to the heart, the more elastin and the farther away the more smooth muscle. Regardless, wall thickness tends to increase so as to maintain the mean circumferential wall stress on the order of ~150 kPa. Whereas smooth muscle is primarily responsible for synthesizing the extracellular matrix proteins during development, it endows the mature vessel with an ability to constrict or dilate—functions that regulate blood flow locally. Most smooth muscle cells are oriented in the circumferential direction, although in some vessels, they are oriented helically or in the axial direction. Note, too, that smooth muscle hypertrophy (increase in size), hyperplasia (increase in number),

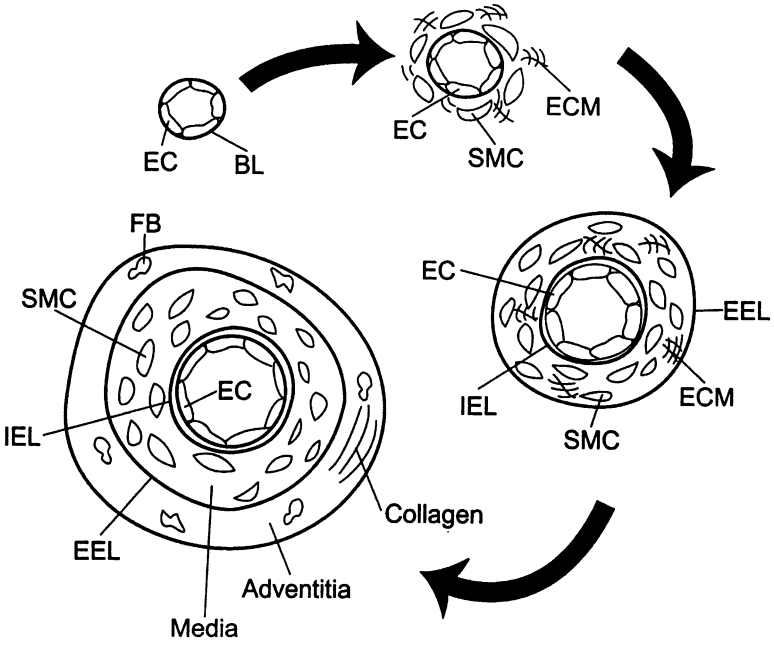

FIGURE 6.17 The three primary layers of the arterial wall: The inner layer, or intima, consists primarily of a monolayer of endothelial cells on a basement membrane; the middle layer, or media, consists largely of smooth muscle with surrounding elastin, collagen, and proteoglycans; the outer layer, or adventitia, consists primarily of collagen with abundant fibroblasts, nerves, and, in some vessels, a small vascular network called the vasa vasorum. Vascular development is seen to begin with endothelial cells (EC) on a basement layer (BL), with smooth muscle cells (SMC) attracted to the abluminal side of the BL, where they replicate and produce significant extracellular matrix (ECM). The adventitia, with abundant fibroblasts (FB), is added last. IEL and EEL denote the internal elastic lamina and the external elastic lamina, respectively, which demarcate the media in most large vessels.

apoptosis (cell suicide), and migration play especially important roles in diseases such as aneurysms, atherosclerosis, and hypertension. Loss of matrix proteins, particularly elastin, similarly plays an essential role in the formation of aneurysms or vascular dissections. Finally, large vessels have an adventitial layer that connects with the perivascular tissue. The adventitia consists primarily of fibroblasts and axially oriented type I collagen, but also includes admixed elastic fibers, nerves and its own small vasculature, the vasa vasorum. The fibroblasts are responsible for regulating the matrix, particularly the collagen. It is thought that the adventitia serves, in part, as a protective sheath that prevents overdistension of the media (like all muscle, smooth muscle contracts maximally at a certain length, above and below which the contractions are less forceful). In summary, most arteries appear to have the same structural motif:

a central parenchymal layer delimited by biologically or structurally important "membranes," the intima and adventitia. Although a detailed understanding of wall mechanics will require detailed modeling of the different properties of these layers and, indeed, the individual constituents within a layer, let us now consider a simple introduction to quantification.

6.5.2 *Theoretical Framework*

Like many other soft tissues, normal arteries often exhibit a nonlinear, pseudoelastic, heterogeneous, and anisotropic behavior over large physiologic strains. Moreover, they tend to behave incompressibly in many cases. It can be shown that in the case of incompressibility, the general constitutive equation embodied in Eq. (6.23) must be modified. For example, for incompressible behavior, we have

$$[\sigma] = -p[I] + [F]\left[\frac{\partial W}{\partial E}\right][F]^T, \tag{6.76}$$

where p is a scalar, pressure-like quantity (actually a Lagrange multiplier) that enforces the incompressibility constraint. That the $-p[I]$ contribution is needed is seen easily by noting that the second term on the right-hand side of Eq. (6.76) represents the stress due to deformation, which is zero in the absence of a deformation.

Imagine then a cube of incompressible material subjected to a hydrostatic pressure P (Fig. 6.18). Clearly, $\sigma_{11} = -P$, $\sigma_{22} = -P$, and $\sigma_{33} = -P$, with all shear stresses zero with respect to $(x, y, z) \equiv (1, 2, 3)$, even though there is no deformation because of incompressibility. Hence, in this case, and this case alone, the Lagrange multiplier p equals the hydrostatic pressure P and Eq. (6.76) correctly describes the state of stress in the absence of a deformation. For a formal derivation of Eq. (6.76), see Humphrey (2002).

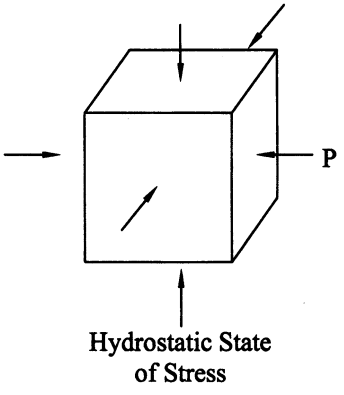

FIGURE 6.18 A small cube of incompressible material subjected to a hydrostatic pressure experiences stress but not strain. Indeed, the components of stress (equal and opposite the pressure) are the same regardless of the coordinate system, (cf. Exercise 2.9).

Now, let us consider the deformation of an artery. Although arteries can have complex geometries (e.g., tapering and bifurcating), we consider here the simplest case: a short, straight, circular, excised segment of uniform thickness. Such samples are commonly tested in the laboratory. Moreover, to simulate in vivo deformations, let us consider a uniform axial extension and inflation via a constant axial load L and pressure P. If we label a generic point in the cross section as (ρ, ϑ, ζ) in an unloaded, excised configuration and (r, θ, z) in an extended and inflated configuration, we can imagine that such a point is extended uniformly by an amount $z = \lambda\zeta$, similar to that in each direction in a biaxial test. Moreover, we might imagine that the deformation is axisymmetric, which is to say, each point may move out radially or axially, but it will maintain its angular position; that is, let $\theta = \vartheta$ Finally, we could relate r to ρ similar to the axial motion (through a constant stretch ratio), but careful consideration suggests that a point on the inner (intimal) surface may displace more radially than a point on the outer (adventitial) surface. Thus, let $r = \widetilde{f}(\rho)$, in general. It can be shown that the deformation gradient $[F]$ associated with this assumed motion,

$$r = \widetilde{f}(\rho), \quad \theta = \vartheta, \quad z = \lambda\zeta, \tag{6.77}$$

is calculated easily and so too the associated stress $[\sigma]$ given a specific form of W. Indeed, there are many reports in the literature from the mid-1960s to the mid-1980s in which this was done. Briefly, these analyses suggested that the circumferential stress $\sigma_{\theta\theta}$ is comparatively much higher in the inner wall than in the outer wall (cf. thick-walled inflation solution in Chap. 3). Indeed, some investigators suggested that this was one cause of atherosclerosis, a disease of the inner wall. In 1983, however, it was noted that the unloaded, excised configuration is not stress-free. In particular, if one introduces a radial cut in such an arterial segment, it "springs open" into a sector. Fung suggested that this revealed the presence of a *residual stress* in arteries that was likely due to differential growth during development. Indeed, Skalak had suggested, in 1981, the possibility of residual stresses due to growth and remodeling. It was Fung and colleagues, however, who demonstrated that vascular adaptations via growth and remodeling processes, such as in hypertension, actually alter this residual stress field. One of the important consequences of residual stress is that it appears to *homogenize* the transmural distribution of stresses within the arterial wall. If this is true, this would suggest that cells at different locations within the wall tend to experience similar stresses under normal conditions. Conversely, altered conditions may render the transmural stress field less homogeneous and thus induce growth and remodeling processes that are different at different spatial locations but that together seek to restore overall normalcy. Quantification of soft tissue growth and remodeling is thus a very important current area of research. Here, however, let us return to the question of wall stress in the normal wall.

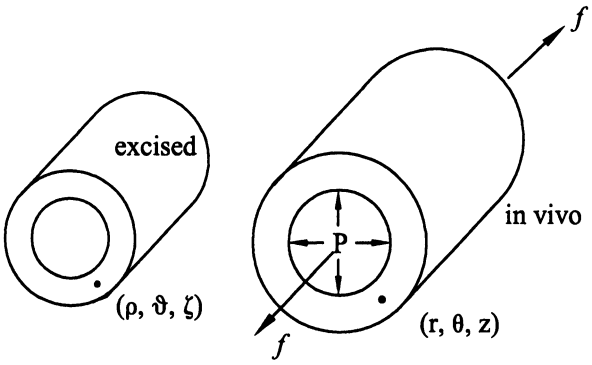

FIGURE 6.19 A segment of an artery that is removed from the body (*left*) and the same segment isolated fictitiously in the body via a free-body diagram.

Figure 6.19 shows two configurations that occur naturally in an experiment on an artery: One is the unloaded, excised cylindrical segment and the other is a fictitious segment associated with the free-body diagram from the in vivo state. Figure 6.20 shows an additional radially cut configuration for which we label our previous generic material point via (R, Θ, Z). It can be shown that the motion from (R, Θ, Z) to (ρ, ϑ, ζ) can be approximated by

$$\rho = g(R), \quad \vartheta = \frac{\pi}{\Theta_0}\Theta, \quad \zeta = \delta Z, \tag{6.78}$$

where Θ_0 is a measure of how much the arterial segment springs open when cut radially and δ is a possible axial extension associated with this cutting process. From Eqs. (6.78) and (6.77), therefore, we see that

$$r = \widetilde{f}(g(R)), \quad \theta = \frac{\pi}{\Theta_0}\Theta, \quad z = \lambda\delta Z, \tag{6.79}$$

or

$$r = f(R), \quad \theta = \frac{\pi}{\Theta_0}\Theta, \quad z = \Lambda Z, \tag{6.80}$$

where $\Lambda \equiv \lambda\delta$. It can be shown (Humphrey 2002) that components of the deformation gradient $[F]$, relative to cylindrical coordinates, can be computed in general via

$$[F] = \begin{bmatrix} \dfrac{\partial r}{\partial R} & \dfrac{1}{R}\dfrac{\partial r}{\partial \Theta} & \dfrac{\partial r}{\partial Z} \\ r\dfrac{\partial \theta}{\partial R} & \dfrac{r}{R}\dfrac{\partial \theta}{\partial \Theta} & r\dfrac{\partial \theta}{\partial Z} \\ \dfrac{\partial z}{\partial R} & \dfrac{1}{R}\dfrac{\partial z}{\partial \Theta} & \dfrac{\partial z}{\partial Z} \end{bmatrix}. \tag{6.81}$$

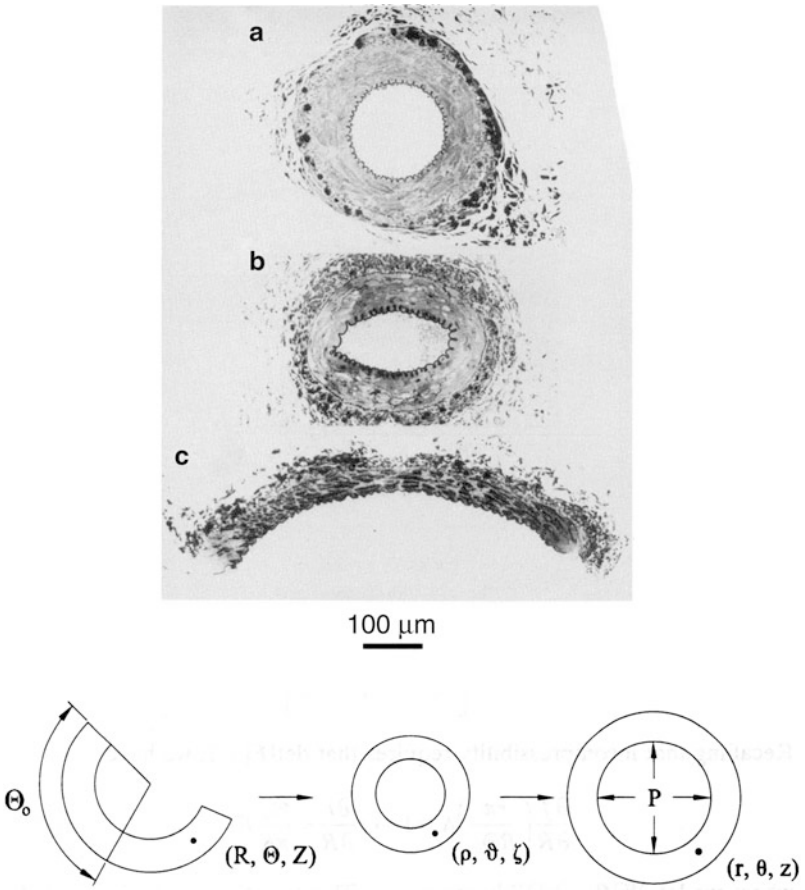

FIGURE 6.20 Three configurations of importance in arterial mechanics: a radially cut unloaded ring, which opens (panel (**c**)), an intact but unloaded ring (panel (**b**)), and an intact and loaded segment (panel (**a**)). The internal elastic lamina is seen to be waviest in the intact, unloaded configuration, consistent with the presence of compressive residual stresses in the inner wall. (From Fung and Liu (1992), reprinted with permission from the American Physiological Society.) The schema below shows coordinate systems for each configuration.

Herein, the derivation of the form for $[F]$ is not critical; rather, we will focus on its use. Nonetheless, note that each term is a nondimensional ratio of a current length to an original length. This is the reason for the presence of the r and R in the circumferential terms—a radius times an angle gives an arc length having units of length rather than radians.

From Eqs. (6.80) and (6.81), therefore, we have for our residually stressed artery,

$$[F] = \begin{bmatrix} \dfrac{\partial f}{\partial R} & 0 & 0 \\ 0 & \dfrac{r\pi}{R\Theta_0} & 0 \\ 0 & 0 & \Lambda \end{bmatrix}. \tag{6.82}$$

Recalling that incompressibility requires that $\det[F] = 1$, we have

$$\frac{\partial f}{\partial R}\left(\frac{r\pi}{R\Theta_0}\right)\Lambda = 1 \rightarrow r\frac{\partial r}{\partial R} = \frac{\Theta_0}{\pi\Lambda}R, \tag{6.83}$$

where we let $\partial f/\partial R \equiv \partial r/\partial R$ because $r \equiv f$. This equation can be integrated,

$$\int_{r_i}^{r} r\frac{\partial r}{\partial R}dR = \int_{R_i}^{R} \frac{\Theta_0}{\pi\Lambda}RdR, \tag{6.84}$$

to yield [because $dr = (\partial r/\partial R)dR$ by the chain rule]

$$r^2 - r_i^2 = \frac{\Theta_0}{\pi\Lambda}\left(R^2 - R_i^2\right) \quad \forall R \in [R_i, R_a], \tag{6.85}$$

where the subscripts i and a denote intimal and adventitial, respectively. Note, therefore, that incompressibility determines the previously unknown form of $r = f(R)$, which is seen to be quadratic in R. Now, the Green strains are determined easily from Eq. (6.7):

$$[E] = \frac{1}{2}\begin{bmatrix} \left(\frac{\Theta_0 R}{\pi\Lambda r}\right)^2 - 1 & 0 & 0 \\ 0 & \left(\frac{r\pi}{R\Theta_0}\right)^2 - 1 & 0 \\ 0 & 0 & \Lambda^2 - 1 \end{bmatrix}, \tag{6.86}$$

from which we see that $E_{RR} \equiv E_{11}$ and $E_{\Theta\Theta} \equiv E_{22}$ are functions of radius, whereas $E_{zz} \equiv E_{33}$, the axial strain, is not.

Fung's orthotropic exponential pseudostrain-energy function W [Eqs. (6.25) and (6.26)] has been shown to describe some arterial behaviors; hence, we will use it here for illustrative purposes. Note, therefore, that in cylindricals (and for principal strains), it is

$$W = \frac{1}{2}c\left(e^Q - 1\right), \tag{6.87}$$

with

$$Q = c_1 E_{RR}^2 + c_2 E_{\Theta\Theta}^2 + c_3 E_{ZZ}^2 + 2c_4 E_{RR} E_{\Theta\Theta} + 2c_5 E_{\Theta\Theta} E_{ZZ} + 2c_6 E_{ZZ} E_{RR}. \tag{6.88}$$

Hence, our nonzero components of Cauchy stress are, from Eq. (6.76),

$$\sigma_{rr} = -p + \left(\frac{\Theta_0 R}{\pi \Lambda r}\right)^2 \frac{\partial W}{\partial E_{RR}}, \tag{6.89}$$

$$\sigma_{\theta\theta} = -p + \left(\frac{r\pi}{R\Theta_0}\right)^2 \frac{\partial W}{\partial E_{\Theta\Theta}}, \tag{6.90}$$

$$\sigma_{ZZ} = -p + (\Lambda)^2 \frac{\partial W}{\partial E_{ZZ}}, \tag{6.91}$$

where the requisite partial derivatives are computed easily from Eqs. (6.87) and (6.88). Now, let us turn to the equilibrium equations. First, however, note that the deformation depends only on the radial direction. In the absence of body forces, Eqs. (3.11)–(3.13) (equilibrium in cylindrical coordinates) reduce to

$$\frac{d\sigma_{rr}}{dr} + \frac{\sigma_{rr} - \sigma_{\theta\theta}}{r} = 0, \quad -\frac{\partial p}{\partial \theta} = 0, \quad -\frac{\partial p}{\partial z} = 0, \tag{6.92}$$

the last two of which reveal that the Lagrange multiplier p, like the deformation, depends on r at most. Our only nontrivial equilibrium equation thus becomes

$$\frac{d\sigma_{rr}}{dr} = \frac{\sigma_{\theta\theta} - \sigma_{rr}}{r}, \tag{6.93}$$

which can be integrated as

$$\int \frac{d\sigma_{rr}}{dr} dr = \int \left(\frac{\sigma_{\theta\theta} - \sigma_{rr}}{r}\right) dr. \tag{6.94}$$

Depending on our prescription of the integration limits, this equation allows us to determine either the transmural pressure P or the Lagrange multiplier. For the first, consider

$$\int_{r_i}^{r_a} \frac{d\sigma_{rr}}{dr} dr = \sigma_{rr}(r_a) - \sigma_{rr}(r_i) = \int_{r_i}^{r_a} \left(\frac{\sigma_{\theta\theta} - \sigma_{rr}}{r}\right) dr \tag{6.95}$$

or

$$P_i - P_a \equiv P = \int \left(\frac{\sigma_{\theta\theta} - \sigma_{rr}}{r}\right) dr, \tag{6.96}$$

given stress boundary conditions that $\sigma_{rr}(r_i) = -P_i$ and $\sigma_{rr}(r_a) = -P_a$, the intimal and adventitial pressure, respectively. Conversely, consider

$$\int_{r_i}^{r} \frac{d\sigma_{rr}}{dr} dr = \sigma_{rr}(r) - \sigma_{rr}(r_i) = \int_{r_i}^{r} \left(\frac{\sigma_{\theta\theta} - \sigma_{rr}}{r}\right) dr \tag{6.97}$$

whereby σ_{rr} is given by Eq. (6.89) and thus

$$-p(r) + \left(\frac{\Theta_0 R}{\pi \Lambda r}\right)^2 \frac{\partial W}{\partial E_{RR}} + P_i = \int_{r_i}^{r} \left(\frac{\sigma_{\theta\theta} - \sigma_{rr}}{r}\right) dr \tag{6.98}$$

allows one to determine p as a function of r. Finally, note that in either case, for the Fung exponential, Eqs. (6.89) and (6.90) allow us to compute

$$\int \left(\frac{\sigma_{\theta\theta} - \sigma_{rr}}{r}\right) dr = \int \left[\left(\frac{r\pi}{R\Theta_0}\right)^2 \frac{\partial W}{\partial E_{\Theta\Theta}} - \left(\frac{\Theta_0 R}{\pi \Lambda r}\right)^2 \frac{\partial W}{\partial E_{RR}}\right] \frac{dr}{r}, \tag{6.99}$$

where

$$\frac{\partial W}{\partial E_{\Theta\Theta}} = ce^{Q}(c_2 E_{\Theta\Theta} + c_4 E_{RR} + c_5 E_{ZZ}), \tag{6.100}$$

$$\frac{\partial W}{\partial E_{RR}} = ce^{Q}(c_1 E_{RR} + c_4 E_{\Theta\Theta} + c_6 E_{ZZ}) \tag{6.101}$$

from Eqs. (6.87) and (6.88), with

$$\begin{aligned} E_{RR} &= \frac{1}{2}\left(\left(\frac{\Theta_0 R}{\pi \Lambda r}\right)^2 - 1\right), \quad E_{\Theta\Theta} = \frac{1}{2}\left(\left(\frac{r\pi}{R\Theta_0}\right)^2 - 1\right), \\ E_{ZZ} &= \frac{1}{2}(\Lambda^2 - 1). \end{aligned} \tag{6.102}$$

Hence, if we know the material properties (c, c_1,..., c_6), the residual stress related opening angle Θ_0 and extension δ, the radially cut dimensions R_i and R_a, the stretch λ and either r_i, or P, then we can solve for the stresses. The associated integrals are obviously complex but can be evaluated easily via numerical methods such as Simpson's rule or more sophisticated methods such as the Romberg method or a Gauss quadrature.

6.5.3 *Illustrative Results*

Panel a in Fig. 6.21 shows predicted transmural stresses for the case in which we ignore the residual stress (i.e., assume $\Theta_0 = \pi$ and $\delta = 1$) but let $\lambda = 1.8$ and $P = 120$ mmHg. Note the steep gradients in stress, which, as noted earlier,

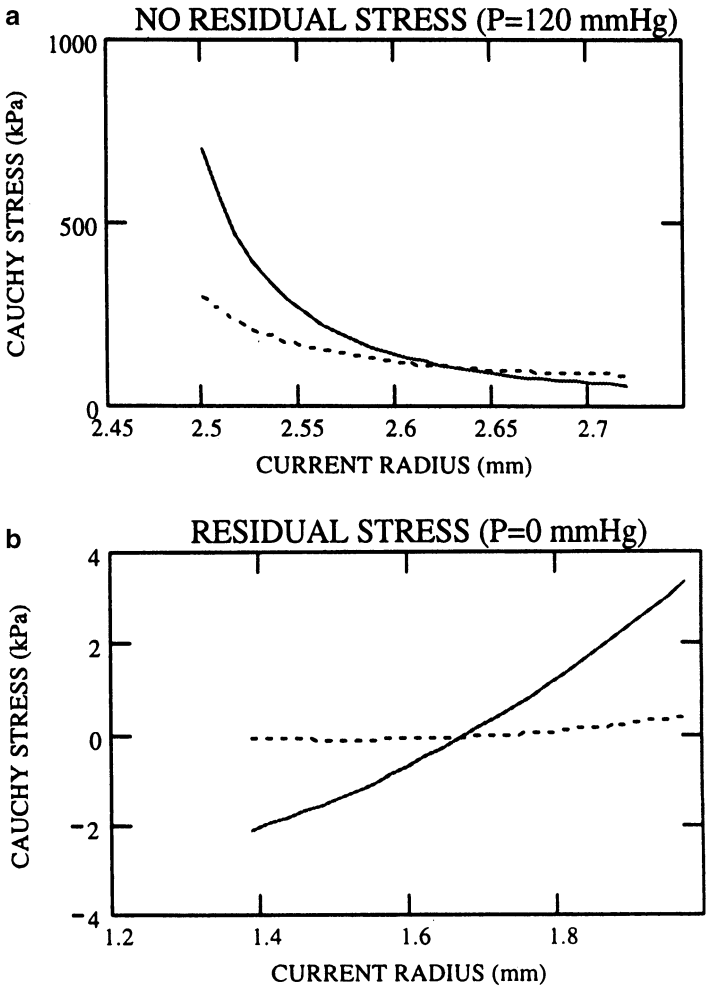

FIGURE 6.21 Panel (**a**): Predicted transmural distribution of stresses (*solid line* is circumferential stress and *dashed line* is axial stress) when one neglects the effects of residual stress and smooth muscle activation. Panel (**b**): Computed residual stresses alone. Note the different orders of magnitude in the stresses in the two panels and the compression in the inner wall in Panel (**b**) consistent with the histology in Figure 6.20. The following values of the parameters were used in the computations: $c = 22.4$ kPa, $c_1 = 0.0499$, $c_2 = 1.0672$, $c_3 = 0.4775$, $c_4 = 0.0042$, $c_5 = 0.0903$, and $c_6 = 0.0585$, whereas, $R_i = 3.92$ mm, $R_a = 4.52$ mm, $\delta = 1.0177$, and $\lambda = 1.767$.

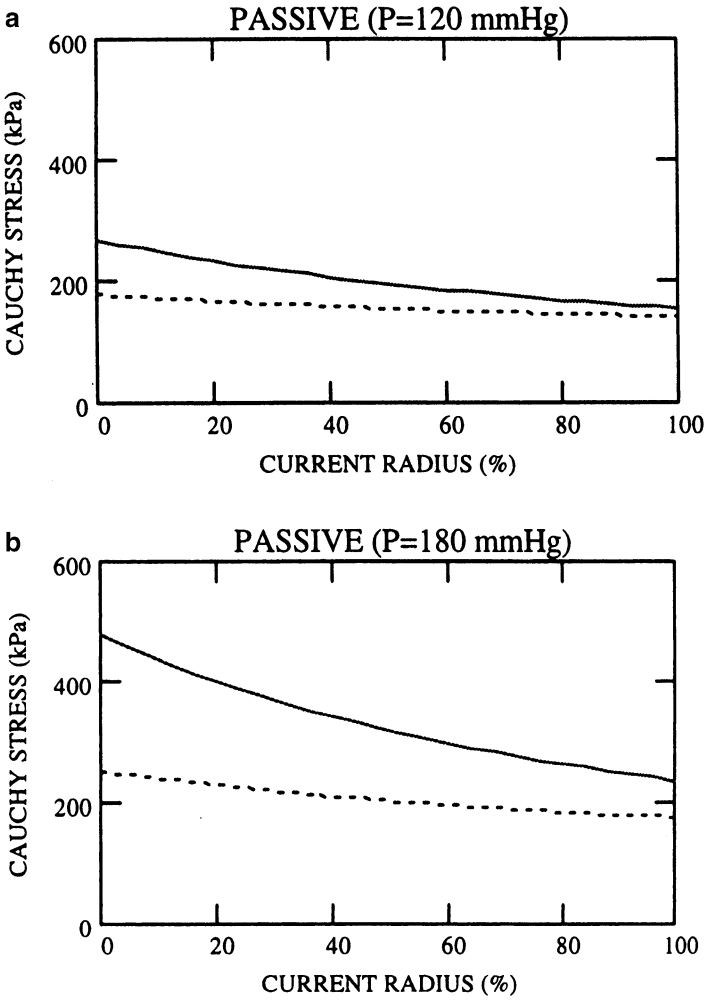

FIGURE 6.22 Panel (**a**): Predicted transmural distribution of stress when residual stress is accounted for; in comparison to Panel (**a**) in Fig. 6.21, inclusion of the residual stress tends to reduce and homogenize the stresses. Panel (**b**): Despite the presence of residual stress, high blood pressure (acute hypertension) would tend to increase the stresses and their transmural gradients in the absence of any functional adaptation. Such deviations from normal values could set into motion various growth and remodeling processes.

suggested to some that atherosclerosis occurs because of large intimal stresses. Panel a in Fig. 6.22 shows, however, that these predicted stresses are much closer to a homogenous distribution if one includes the residual stress, here with $\Theta_0 = 71.4^\circ$ and $\delta = 1.017695$ (Humphrey 2002). One of the remarkable things revealed by this (simple) nonlinear analysis is that inclusion of residual stress

reduces the computed stresses many fold despite the residual stresses [based on deformations from (R, Θ, Z) to (ρ, ϑ, ζ) only] actually being very small in magnitude, ~3 kPa (panel b in Fig. 6.21). This dramatic effect is due solely to the material and kinematic nonlinearities, which would simply be missed with a linear analysis [cf. Eq. (3.80)]. Moreover, it is clear that the principle of superposition of Sect. 5.5 of Chap. 5 does not hold in this case; subtracting a circumferential residual stress of ~3 kPa from those in Fig. 6.21a clearly does not yield the computed values in Fig. 6.22a. The full nonlinear analysis is thus essential here as in most problems in soft tissue biomechanics and likely cell mechanics.

In conclusion, we emphasize that this analysis was presented simply to illustrate some of the unique aspects of a nonlinear stress analysis and to provide a glimpse into methods used in cardiovascular mechanics and other areas of soft tissue mechanics. This presentation—even for a straight uniform segment—was simplified, however, for we did not consider the heterogeneity of the composition of the wall (i.e., different behavior of the media and adventitia) or the dynamical loading due to pulsatile flow. These and other effects are addressed in Humphrey (2002). Nevertheless, even in that text, the analysis is simplified. There is much more to learn about the mechanics of blood vessels, their basic constitutive relations, especially for smooth muscle, their variations in properties along the length of a vessel or through a bifurcation, their changes due to growth and remodeling, and so on. To advance our understanding in these areas, we must not only apply mechanics, but we must also develop and extend it. The challenge is great, but so is the need.

Observation 6.3. Amongst the many proteins, glycoproteins, and glycosaminoglycans that contribute to the structural integrity of arteries, elastic fibers are unique. Briefly, functional fibers are produced primarily during the perinatal period and they consist of the protein elastin (~90 %) and associated glycoproteins (e.g., fibrillins and fibulins). Unique desmosine and isodesmosine based cross-links render elastic fibers the most biologically and thermally stable structural constituent within the arterial wall. In humans, for example, the half-life of elastic fibers under normal conditions is 50+ years.

Elastic fibers tend to be organized into fenestrated sheets, or laminae, within the arterial wall. Most muscular arteries (e.g., coronary or renal arteries, but not cerebral arteries) have two prominent elastic layers, the internal elastic lamina (IEL) and external elastic lamina (EEL), which demarcate the intimal and medial layers and the medial and adventitial layers, respectively (cf. Fig. 6.17). Elastic arteries, which are found closer to the heart (e.g., the aorta), have many concentric laminae, each of which separates layers of smooth muscle cells, collagens, and glycosaminoglycans. Multiple genetic mutations lead to defects in the elastic fibers, which in turn compromise the function or structural integrity of the wall.

Williams Syndrome results from a defect in the gene coding elastin; these patients tend to present with supravalvular aortic stenosis. In contrast, Marfan Syndrome results from a defect in the gene coding fibrillin-1; these patients tend to develop thoracic aortic aneurysms and dissections, often at a young age. It is interesting, therefore, that defects that ultimately affect the same constituent of the extracellular matrix, elastic fibers, can give rise either to a narrowing of an artery (stenosis) or a dilatation (aneurysm). To understand such different manifestations, one must understand both the biology and the mechanics.

It appears, for example, that properly cross-linked elastin in development provides important biological cues to adjacent smooth muscle cells to be quiescent and contractile. Without these cues, these cells may proliferate and migrate inward, hence resulting in a focal or diffuse narrowing. In contrast, association of fibrillin-1 with elastin appears to contribute significantly to the long-term mechanical, and perhaps biological, stability of elastic fibers. In cases of reduced or non-functional fibrillin-1, arterial elastic fibers appear to be more susceptible to both fatigue-induced mechanical damage (recalling that the human heart beats, on average, ~31.5 million cycles per year) and proteolytic degradation. It is also important to note that fibrillin-1 not only has an important mechanical role, it also serves an important biological role by sequestering latent transforming growth factor—beta (TGF-β) within the extracellular matrix. Lack of sequestration can lead to an increased activity of TGF-β and a host of downstream consequences, including altered cellular behaviors and matrix turnover. There is, therefore, a pressing need to understand both the biological and mechanical implications of genetic mutations of extracellular matrix, particularly in tissues and organs that serve a mechanical role. See the excellent review article by Wagenseil and Mecham (2012) for more on arterial elastin.

6.6 A Role of Vascular Smooth Muscle

6.6.1 Muscle Basics

Although we only considered the passive (i.e., noncontracting) mechanical behavior of arteries in Sect. 6.5, the role of smooth muscle activation is fundamental to vascular function. Vascular smooth muscle constitutes 40–60 % (by dry weight) of the medial portion of muscular and resistive blood vessels. It is responsible for maintaining a "basal tone," which, in turn, allows the vessel to vasoconstrict or vasodilate as needed to control local blood flow. Such regulation is fundamental, for example, for diverting blood to muscles during exercise, to the digestive system following eating, or away from the skin to minimize heat transfer when the external temperature is low.

Like all muscle (e.g., skeletal and cardiac), contraction of vascular smooth muscle depends on the concentration of intracellular free calcium and a sliding

filament, cross-bridge-mediated mechanics (Chap. 1). The steady-state cytoplasmic calcium is maintained primarily via a calmodulin-regulated Ca-ATPase activity. Sources of calcium include the intracellular sarcoplasmic reticulum and transmembrane influx from the extracellular milieu; a rise in cytoplasmic free calcium triggers a contraction. Despite the similarities, vascular smooth muscle differs from skeletal and cardiac muscle in numerous ways. Smooth muscle has a much higher ratio of actin to myosin, and the actin–myosin complexes are not arranged in sarcomeres, as they are in striated muscle. Smooth muscle can also shorten more than striated muscle, albeit at a much lower rate, and it can maintain its maximum contraction at a steady level for much longer periods and at a lower energy expenditure than striated muscle. Finally, whereas striated muscle generates its greatest force at a length where the passive stress is nearly zero, smooth muscle generates its greatest force at a length where the passive stress is significant (Fig. 6.23). The ability to generate force (or stress) also depends on the contractile state, which can be governed by the concentration of a particular agonist like the neurotransmitter norepinephrine (NE). An associated sigmoidal dose–response curve is illustrated in Fig. 6.24; that is, active force generation essentially increases with the concentration of the agonist once a threshold is exceeded, but force generation does not increase beyond a saturation value of the agonist.

6.6.2 *Quantification*

Despite its fundamental importance and despite the cross-bridge mechanism being proposed nearly 50 years ago (1954), we still do not have a widely accepted mathematical descriptor for active stress generation. Indeed, perhaps one of the greatest unknowns in biomechanics is the *multiaxial character* of muscle activation. Historically, muscle has been thought to generate stress only in the direction of the long axis of the actin–myosin complex (i.e., is one

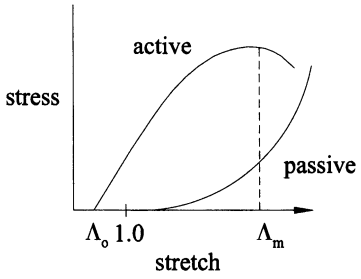

FIGURE 6.23 Schema of the length—tension response of vascular smooth muscle. This response is similar to that in skeletal muscle, with the exception that the passive tension is significant in smooth muscle at that value of stretch where the active force generation is largest.

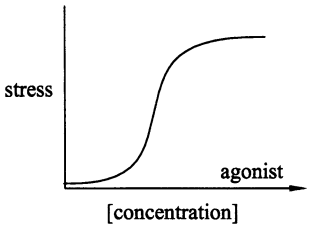

FIGURE 6.24 Dose–response curve for vascular smooth muscle. The concentration of the agonist could range from 10^{-7} to 10^{-4} for a typical test using norepinephrine (NE), a vasoconstrictor.

dimension). We now know that muscle activation is multiaxial, but the data and theory needed for quantification remain lacking. Here, therefore, let us consider the current state of the art.

It is generally assumed that the passive and active contributions to the stress are additive; thus, $\sigma = \sigma^p + \sigma^a$, where the superscripts p and a denote passive and active. Moreover, the smooth muscle is oriented in the circumferential direction in most blood vessels; hence, it is generally assumed that

$$\sigma_{rr} \equiv \sigma^p_{rr}, \quad \sigma_{\theta\theta} = \sigma^p_{\theta\theta} + \sigma^a_{\theta\theta}, \quad \sigma_{zz} \equiv \sigma^p_{zz}. \tag{6.103}$$

Perhaps the best currently available relation for the active component of stress is that proposed in 1999 by Rachev and Hayashi (see Chap. 7 in Humphrey 2002). It can be written as

$$\sigma^a_{\theta\theta} = T_0\left(\mathrm{Ca}^{2+}\right)\Lambda_\theta\left[1 - \left(\frac{\Lambda_m - \Lambda_\theta}{\Lambda_m - \Lambda_0}\right)^2\right], \tag{6.104}$$

where T_0 has units of stress and represents the dose–response dependency on cytoplasmic free calcium. The second part of this relation represents the stretch-dependent stress generation, where Λ_θ is the stretch in the circumferential direction, Λ_0 is the minimum value of stretch where no stress generation is possible, and Λ_m is that value of stretch where the active stress generation is maximum. Typical values of Λ_0 and Λ_m are 0.6–0.8 and 1.5–1.75, respectively. Note, too, that $T_0 \sim 50$ kPa for a basal tone, but it can range from 0 to ~100 kPa. From Sect. 6.5, we see that $\Lambda_\theta = r\pi/R\Theta_0$ where Θ_0 is the residual stress related opening angle and r and R are radii in the current and original (stress-free) configurations, respectively.

Recall from the previous section that including the effects of residual stress dramatically reduced the computed values of the circumferential stress, particularly in the inner wall, and its transmural gradient. Rachev and Hayashi showed that including a basal smooth muscle tone further reduces the computed

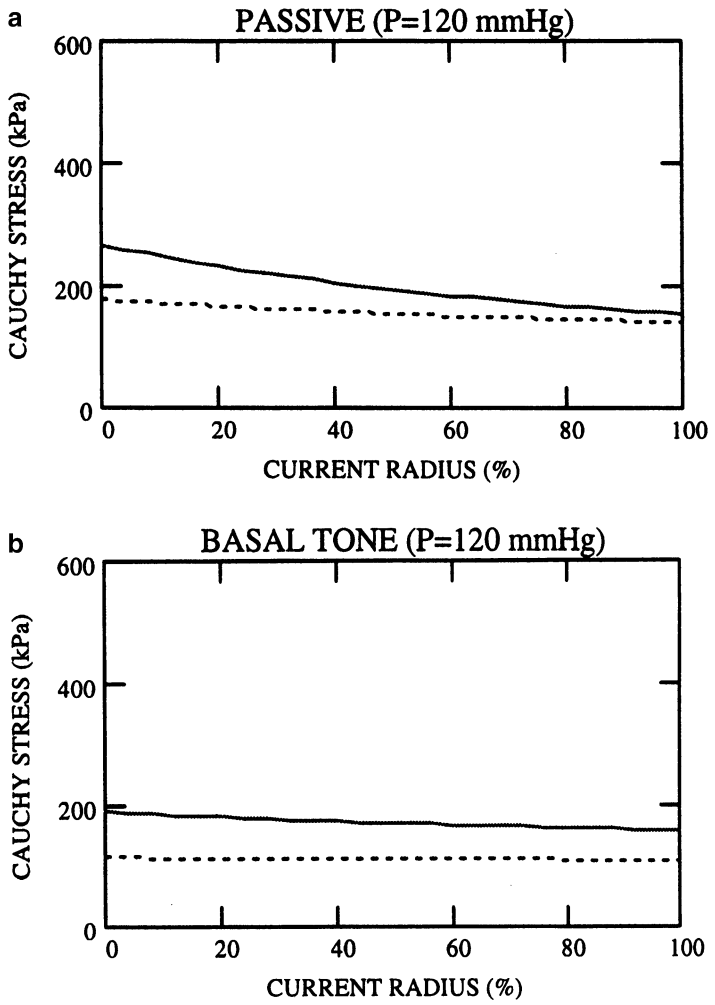

FIGURE 6.25 Panel (**a**): We repeat panel (**a**) from Fig. 6.22 to compare it directly to the case when a basal tone (i.e., smooth muscle activation modeled via $T_0 = 50$ kPa) is included in the analysis (Panel (**b**)). It is seen that smooth muscle activation tends to reduce the stresses and their gradients.

circumferential stress and its gradient (compare panels a and b in Fig. 6.25). Hence, it appears that a basal smooth muscle tone not only allows vasoconstriction or vasodilation as needed, it also modifies the normal stiffness of the wall and thereby helps to homogenize the transmural distribution of stress. A homogenous stress field in normalcy seems reasonable teleologically because each cell would experience the same baseline mechanical environment.

Of course, disease, injury, and clinical intervention (e.g., balloon angioplasty) can perturb the mechanical environment, which, via mechanotransduction

mechanisms, tends to set into motion various growth and remodeling responses that seek to restore normalcy or at least to arrest the damage or insult. As noted earlier, modeling biological growth and remodeling is one of the most important and exciting areas of research in biomechanics today. It is, however, mathematically complex and beyond an introductory text. We merely discuss a few of the basics of vascular growth and remodeling in Sect. 11.1.

In closing, however, let us see how an abrupt change in blood pressure can increase the value and gradients of the transmural stresses and how an immediate vasoactive response can tend to restore the stresses *toward* normal values; full restoration requires growth and remodeling, however. Whereas panel b in Fig. 6.25 shows stresses at $P = 120$ mmHg, panel a in Fig. 6.26 shows values for the same artery at 180 mmHg with the same basal tone. The rise in stress is due largely to the distention of the vessel and the associated stretching of the nonlinear passive components of the wall. Indeed, a vasodilatation (panel b in Fig. 6.22) allows a further distension and thus exacerbates the pressure-induced increase in wall stress. Conversely, a vasoconstriction (panel b in Fig. 6.26, with $T_0 = 100$ kPa rather than 50 kPa) tends to reduce the wall stresses toward their original values. Hence, vasoconstriction may be one early mechanism that the blood vessel uses to combat hypertension. Again, however, the detailed mechanics are very complex and the reader is referred to Humphrey (2002) and the archival literature for more details. Indeed, this chapter was but a brief introduction to the nonlinear mechanics of tissues and cells, hopefully an appetizer that has stimulated the reader's desire to learn more and to explore more deeply this important and fascinating area of research.

Chapter Summary

Nonlinearities manifest in many areas of biomechanics, particularly in constitutive responses and in the finite strains and rotations experienced by many cells, tissues, or organs. The latter is evident in the heart, for example, which experiences complex finite strains and rotations upon every contraction. Section 6.1 revealed important restrictions of the linearized strain ε that was used throughout Chaps. 2–5 (and which restricted many of the associated solutions) whereas Sect. 6.2 presented both a nonlinear stress—stretch relation that is commonly used in soft tissue mechanics and a clever method introduced by Y.C. Fung to obtain such a relation directly from data. Indeed, one of the most important realizations is that linear relationships can be defined uniquely (e.g., $y = mx + b$, where m is the slope and b the intercept) whereas nonlinear relationships cannot be so defined. There is need, therefore, for clever, theoretically motivated experiments for formulating nonlinear constitutive relations, one of the greatest challenges in biomechanics today.

Because of the *finite deformations* experienced by many cells, tissues, and organs, we found that multiple definitions of stress (e.g., Cauchy versus first or

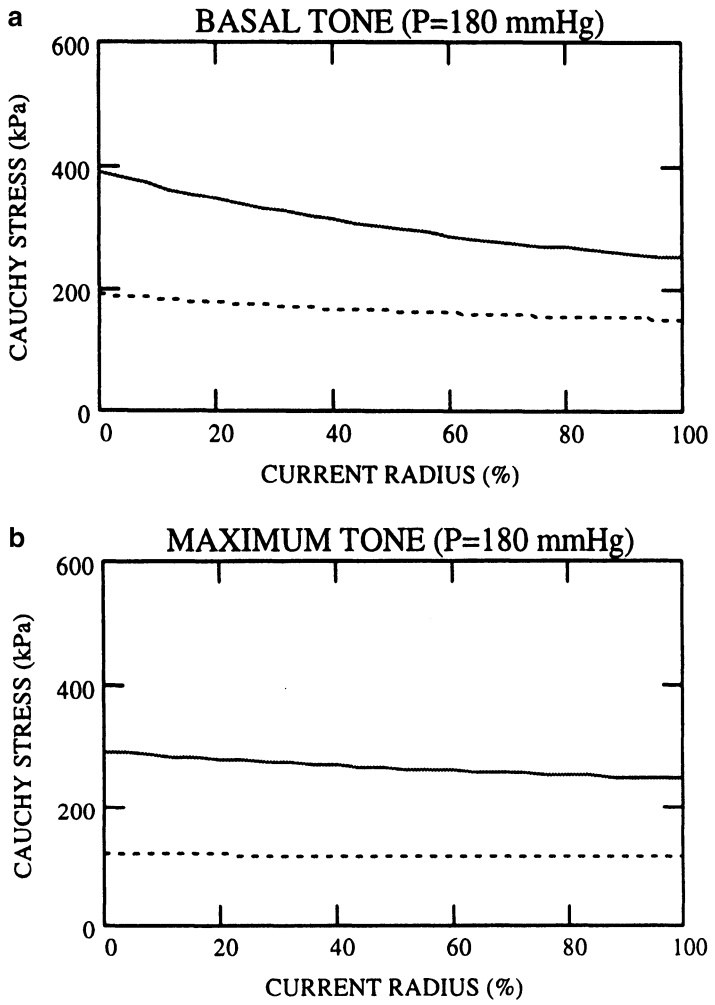

FIGURE 6.26 Panel (**a**): Transmural stress distribution at high blood pressure when the smooth muscle is at its basal tone. Compared to Fig. 6.22b, we see that a basal smooth muscle activation tends to decrease the stresses from those in the passive state alone. Indeed, panel (**b**) shows that further activation ($T_0 = 100$ kPa rather than the 50 kPa in the basal case) tends to decrease the stresses in the case of high blood pressure. It seems reasonable to hypothesize, therefore, that an augmented smooth muscle activation may be an early response of large vessels to hypertension. Because the stresses are not restored to normal values and because of the increased energetic demand of fully contracted muscle, however, subsequent growth and remodeling would be expected. This is consistent with the observation that hypertensive vessels tend to thicken over time via an increase in both smooth muscle and extracellular matrix, especially collagen.

second Piola-Kirchhoff) and strain (e.g., Green versus linearized) are both possible and useful. There is a need to understand well the different definitions and their uses. In general, in solid mechanics the Cauchy stress is useful in analytical analyses, the first Piola-Kirchhoff stress is useful in experimental studies, and the second Piola-Kirchhoff stress is useful in constitutive formulations. The illustrative analysis of the in-plane stretching of a thin slab of elastomer or soft tissue in Sect. 6.3 is thus important for it reveals an analysis that is fundamental to the interpretation of a common experiment in soft tissue biomechanics and it provides a simple intuitive situation for comparing multiple definitions of stress and their separate utilities. Indeed, it is always good to appreciate new concepts via simple problems, which in turn builds confidence when seeking to understand more complex situations using the same general approach.

The general concept of stability introduced via the study of column buckling in Chap. 5 was extended here to a clinically relevant and challenging problem (neuroangioplasty) wherein the inherent nonlinearities were retained to enable study of both *stable* and *unstable* paths. The interested reader is encouraged to research the history of this particular problem whereby he or she will discover that an adverse clinical observation (instability of the neuroangioplasty balloon) could have been anticipated and controlled had the appropriate nonlinear analysis been performed during the research and development stage. Moreover, because such instabilities were well known in the rubber elasticity literature, it reminds us that we should be well read in related areas. By way of foreshadowing, this analysis of stability is extended in Chap. 11 to include solid–fluid interactions that are important in the dynamical stability of intracranial aneurysms.

Finally, we studied one implication of a *residual stress* field, which was an important discovery in the mid-1980s, and we illustrated one method for its calculation. Whereas much more detail can be found in Humphrey (2002), we showed that deformations experienced by a radially cut, excised segment of artery (Fig. 6.20) can be described via *multiplicative finite deformations*, and that a particular 3-D constitutive relation for arterial behavior (Eq. 6.87) is merely an extension of the 1-D Fung-elastic relation derived in Sect. 6.2. Most importantly, however, we found that the existence of residual stresses in a thick-walled artery (Fig. 6.21) tends to homogenize the transmural stress field in vivo (Fig. 6.22a), which in turn motivated a *fundamental hypothesis of mechanobiology* (Humphrey 2008)—that cells tend to establish, maintain, and restore a preferred (homeostatic) mechanical environment. In this case, therefore, we see how a fundamental solution of biomechanics actually gave rise to an important biological hypothesis, which reminds us that mechanics can and should be much more than a means of computing values of stress or strain and predicting possible material failure.

Appendix 6: Matrices

A matrix is a mathematical device that is useful for manipulating arrays of numbers (or variables). In general, a $m \times n$ matrix is written with m rows of entries and n columns; it is convention to enclose these entries within brackets [ ]. For example, a 2×2 matrix has four entries, given by two rows and two columns, represented as

$$[A] = \begin{bmatrix} A_{11} & A_{12} \\ A_{21} & A_{22} \end{bmatrix}, \tag{A6.1}$$

from which we see that the indices denote the (row, column). Hence, the ith row, jth column entry can be denoted as A_{ij} (i.e., for stress, rows represent faces and columns the directions). Accepted *rules* govern the addition, subtraction, and multiplication of matrices. For example, two matrices $[A]$ and $[B]$ can be added or subtracted *if and only if* they have the same number of rows and columns. A 2×2 matrix can thus be added to another 2×2 matrix, but it cannot be added to a 3×3 matrix. In the former case, we have

$$\begin{aligned} [A] \pm [B] &= \begin{bmatrix} A_{11} & A_{12} \\ A_{21} & A_{22} \end{bmatrix} \pm \begin{bmatrix} B_{11} & B_{12} \\ B_{21} & B_{22} \end{bmatrix} \\ &= \begin{bmatrix} A_{11} \pm B_{11} & A_{12} \pm B_{12} \\ A_{21} \pm B_{21} & A_{22} \pm B_{22} \end{bmatrix}, \end{aligned} \tag{A6.2}$$

which is to say, addition and subtraction are accomplished by simply adding or subtracting like entries.

Matrix multiplication is much different. Two matrices can be multiplied *if and only if* the number of columns of the first matrix equal the number of rows of the second matrix. Thus, a $m \times n$ matrix cannot be multiplied by a $m \times n$ matrix if $m \neq n$. Rather, a $m \times p$ matrix must multiply a $p \times n$ matrix ($m = n$ allowed but not required) whereby we find that the resulting number of rows and columns of the product matrix is $(m \times p) \times (p \times n) = m \times n$. For example, if

$$[C] = \begin{bmatrix} C_{11} & C_{12} \\ C_{21} & C_{22} \\ C_{31} & C_{32} \end{bmatrix}, \quad [B] = \begin{bmatrix} B_{11} & B_{12} \\ B_{21} & B_{22} \end{bmatrix}, \tag{A6.3}$$

then we expect $(3 \times 2) \times (2 \times 2) = 3 \times 2$, namely

$$[C][B] = \begin{bmatrix} C_{11}B_{11} + C_{12}B_{21} & C_{11}B_{12} + C_{12}B_{22} \\ C_{21}B_{11} + C_{22}B_{21} & C_{21}B_{12} + C_{22}B_{22} \\ C_{31}B_{11} + C_{32}B_{21} & C_{31}B_{12} + C_{32}B_{22} \end{bmatrix}, \tag{A6.4}$$

from which we see that each row of $[C]$ multiplies each column of $[B]$.

In addition to operations such as addition and multiplication, matrix methods introduce new operations such as the transpose and inverse. The transpose of a matrix, denoted by the superscript T, such as, transpose $([C]) \equiv [C]^T$, is computed by exchanging rows and columns. For example,

$$[C] = \begin{bmatrix} C_{11} & C_{12} \\ C_{21} & C_{22} \\ C_{31} & C_{32} \end{bmatrix} \rightarrow [C]^T = \begin{bmatrix} C_{11} & C_{21} & C_{31} \\ C_{12} & C_{22} & C_{32} \end{bmatrix}, \tag{A6.5}$$

which reveals that $(m \times n)^T = n \times m$. At this point, note that matrices can have a single row or a single column. These are often called "vectors," because the associated entries can represent components of a vector in an n-space. For example, $n \times 1$ and $1 \times n$ matrices, with $n = 3$ as in Euclidean 3-space, can be written as

$$[X] = \begin{bmatrix} X_1 \\ X_2 \\ X_3 \end{bmatrix}, \quad [Y] = [X]^T = [X_1 \quad X_2 \quad X_3]. \tag{A6.6}$$

Hence,

$$[X]^T[X] = [X_1 \quad X_2 \quad X_3] \begin{bmatrix} X_1 \\ X_2 \\ X_3 \end{bmatrix} = \left[X_1^2 + X_2^2 + X_3^2\right], \tag{A6.7}$$

revealing that a 1×1 matrix also exists, which, of course, can represent the value of a scalar. Note, too, that $(1 \times 3) \times (3 \times 1) = (1 \times 1)$, whereas $(3 \times 1) \times (1 \times 3) = (3 \times 3)$, namely

$$\begin{bmatrix} X_1 \\ X_2 \\ X_3 \end{bmatrix} [X_1 \quad X_2 \quad X_3] = \begin{bmatrix} X_1^2 & X_1X_2 & X_1X_3 \\ X_2X_1 & X_2^2 & X_2X_3 \\ X_3X_1 & X_3X_2 & X_3^2 \end{bmatrix}, \tag{A6.8}$$

thus revealing that matrix multiplication does *not* commute in general.

A matrix can be multiplied or divided by a scalar, such as $a[A] = [B]$, where

$$a \begin{bmatrix} A_{11} & A_{12} \\ A_{21} & A_{22} \end{bmatrix} = \begin{bmatrix} aA_{11} & aA_{12} \\ aA_{21} & aA_{22} \end{bmatrix} = \begin{bmatrix} B_{11} & B_{12} \\ B_{21} & B_{22} \end{bmatrix}, \tag{A6.9}$$

and likewise for scalar division. Hence, a scalar acts on each entry individually. This property allows one to factor out common values, such as the 1/2 in the definition of the Green strain $[E]$ in terms of the deformation gradient $[F]$, as in Eq. (6.7).

Whereas a matrix can be multiplied or divided by a scalar, and a matrix can be multiplied by another matrix, *a matrix cannot be divided by another matrix*. This is similar, of course, to vector algebra: A vector can be multiplied by a scalar or a vector (e.g., dot or cross products), but a vector cannot be divided by another vector. In the case of matrices, this issue is addressed in part via the inverse operation. The inverse of a matrix, denoted by the superscript -1, is defined such that

$$[A]^{-1}[A] = [I] = [A][A]^{-1}, \tag{A6.10}$$

where $[I]$ is the identity matrix, which has values of 0 in off-diagonal entries and 1 in diagonal entries [cf. Eq. (6.5)]. To illustrate, consider the 2×2 matrix $[A]$. Letting

$$[A] = \begin{bmatrix} A_{11} & A_{12} \\ A_{21} & A_{22} \end{bmatrix}, \quad [I] = \begin{bmatrix} 1 & 0 \\ 0 & 1 \end{bmatrix}, \tag{A6.11}$$

it can be shown that

$$[A]^{-1} = \frac{1}{J}\begin{bmatrix} A_{22} & -A_{12} \\ -A_{21} & A_{11} \end{bmatrix}, \tag{A6.12}$$

where the scalar J (Jacobian) is the determinant of $[A]$ given by

$$J = \det[A] = A_{11}A_{22} - A_{12}A_{21}. \tag{A6.13}$$

Note, therefore, that

$$\begin{aligned} [A]^{-1}[A] &= \frac{1}{A_{11}A_{22} - A_{12}A_{21}}\begin{bmatrix} A_{22} & -A_{12} \\ -A_{21} & A_{11} \end{bmatrix}\begin{bmatrix} A_{11} & A_{12} \\ A_{21} & A_{22} \end{bmatrix} \\ &= \frac{1}{A_{11}A_{22} - A_{12}A_{21}}\begin{bmatrix} A_{22}A_{11} - A_{12}A_{21} & A_{22}A_{12} - A_{12}A_{22} \\ -A_{21}A_{11} + A_{11}A_{21} & -A_{12}A_{21} + A_{22}A_{11} \end{bmatrix} \\ &= \begin{bmatrix} 1 & 0 \\ 0 & 1 \end{bmatrix} = [I], \end{aligned} \tag{A6.14}$$

as desired. In general, if we let A_{ij} represent the ith row, jth column entry, then

$$A_{ij}^{-1} = \frac{\text{cof}\left[A_{ij}\right]}{\det[A]}, \tag{A6.15}$$

where the cofactor of the entry A_{ij} is defined by

$$\text{cof}\left[A_{ij}\right] = (-1)^{i+j} M_{ji}, \tag{A6.16}$$

where M_{ji} is a so-called minor; it is given by the determinant of the entries left after striking out all entries in row i and column j. For example, given Eq. (A6.1), the M_{11} minor is A_{22}, the M_{12} minor is A_{21}, the M_{21} minor is A_{12}, and the M_{22} minor is A_{11}.

Finally, the determinant of $[A]$ is defined by

$$\det[A] = \sum_{j=1}^{n} A_{ij}(-1)^{i+j} M_{ij} \tag{A6.17}$$

for any i.

Although the inverse and determinant can be difficult to compute for large matrices, they are straightforward for 2×2 and 3×3 matrices, which are particularly useful in mechanics to represent 2-D and 3-D states of stress or strain. In cases of larger matrices, computers are essential. Finally, another operation that is useful in matrix methods is the trace, denoted tr, which is simply the sum of the diagonals of a square matrix. For example, for the 2×2 matrix [A] above, we have $\text{tr}[\text{A}] = \text{A}_{11} + \text{A}_{22}$.

Exercises

6.1 Given a motion defined by

$$x = \Lambda_1 X + \kappa_1 Y, \quad y = X + \Lambda_2 Y, \quad z = Z,$$

find $[F]$, $[E]$, and $[\varepsilon]$ and discuss.

6.2 It can be shown (Humphrey 2002) that $\det[F] = 1$ if the deformation is volume conserving (i.e., isochoric). If

$$x = \Lambda X, \quad y = \Lambda Y, \quad z = \beta Z$$

describes an "equibiaxial stretching" of amount Λ in the in-plane (x, y) directions, determine the value of β such that volume is conserved.

6.3 Assuming an isochoric motion (i.e., $\det[F] = 1$), find the value of Λ in terms of β, when

$$x = \beta X + \kappa Y, \quad y = \kappa X + \beta Y, \quad z = \Lambda Z.$$

6.4 It can be shown that in cylindrical coordinates (see Humphrey 2002),

$$[F] = \begin{bmatrix} \dfrac{\partial r}{\partial R} & \dfrac{1}{R}\dfrac{\partial r}{\partial \Theta} & \dfrac{\partial r}{\partial Z} \\ r\dfrac{\partial \theta}{\partial R} & \dfrac{r}{R}\dfrac{\partial \theta}{\partial \Theta} & r\dfrac{\partial \theta}{\partial Z} \\ \dfrac{\partial z}{\partial R} & \dfrac{1}{R}\dfrac{\partial z}{\partial \Theta} & \dfrac{\partial z}{\partial Z} \end{bmatrix}$$

for a particle originally at (R, Θ, Z) that is currently at (r, θ, z), with $r = r(R, \Theta, Z)$, and so forth. Find $[F]$ and $[E]$ for the following specific motion:

$$r = \beta R, \quad \theta = \Theta, \quad z = \Lambda Z,$$

where β and Λ are stretch ratios. Interpret this motion.

6.5 Find the solution to Eq. (6.10) using a direct integration method. Hint: Note that

$$\frac{d\Sigma}{d\Lambda} = \alpha + \beta\Sigma \rightarrow \frac{1}{\alpha + \beta\Sigma}\frac{d\Sigma}{d\Lambda} = 1.$$

6.6 Using the stress–stretch function of the form

$$\Sigma = \frac{\alpha}{\beta}\left(e^{\beta(\Lambda - 1)} - 1\right)$$

and letting values of the parameters be $\alpha = 10$ MPa and $\beta = 2.5$, plot the associated Σ versus Λ and $d\Sigma/d\Lambda$ versus Σ curves. Additionally, plot $\ln \Sigma$ versus Λ (for Λ up to 1.2) and discuss how such information (if Σ and Λ came from an experiment) could be used to find a constitutive function.

6.7 Given the stress–stretch relation $\Sigma = \Sigma(\Lambda)$ in Exercise 6.6, note that the relation is nonlinear in terms of the material parameter β. Because of the exponential relation, however, one may be able to determine the values of α and β from data using a linear instead of a nonlinear least-squares regression. Find the requisite equations for the linear regression. Hint: Use the natural logarithm.

6.8 Use the general solutions for axisymmetric membranes [Eq. (6.58)] to determine the stress resultants (tensions) for the inflation of an elliptical membrane, an approximate example of which is the lens capsule of the eye.

6.9 The neo-Hookean strain energy function W was used in Sect. 6.4 to examine the stability of an elastomeric spherical membrane. This W was written in terms of the in-plane principal components of the Green strain [Eq. (6.63)]. Show that an equivalent form is

$$W = C\big(\Lambda_1^2 + \Lambda_2^2 + \Lambda_3^2 - 3\big),$$

where $E_{11} = \big(\Lambda_1^2 - 1\big)/2$ and so forth. Moreover, note that for a membrane, W is written in terms of in-plane components only. If we enforce incompressibility kinematically, rather than constitutively, then $\det [F] = 1$ requires that $\Lambda_1\Lambda_2\Lambda_3 = 1$ if $[F] = \text{diag}[\Lambda_1,\ \Lambda_2,\ \Lambda_3]$ Rewrite W in terms of Λ_1 and Λ_2 alone.

6.10 In addition to the Fung exponential for a 2-D membrane,

$$W = c\big(e^Q - 1\big), \quad Q = c_1E_{11}^2 + c_2E_{22}^2 + 2c_3E_{11}E_{22},$$

relative to principal directions, another often used relation for bio-membranes is the Skalak, Tozeren, Zarda, Chien (STZC) relation:

$$W = \frac{c}{8}\big\{4\big(E_{11}^2 + E_{22}^2\big) + \Gamma\big[4\big(E_{11}^2 + E_{22}^2\big) + 8E_{11}E_{22} + 16E_{11}^2E_{22} + 16E_{11}E_{22}^2 + 16E_{11}^2E_{22}^2\big]\big\},$$

where c and Γ are material parameters. If

$$E_{11} = \frac{1}{2}\big(\Lambda^2 - 1\big), \quad E_{22} = \frac{1}{2}\big(\Lambda^2 - 1\big),$$

as in the analysis of the neuroangioplasty balloon, show that

$$T_1 = T_2 = T = \frac{c}{2}\big[\Lambda^2 - 1 + \Gamma\Lambda^2\big(\Lambda^4 - 1\big)\big].$$

6.11 Based on the previous exercise, determine if a STZC spherical membrane exhibits a limit point instability in inflation if $c > 0$ and $\Gamma > 0$. Hint: First, show that

$$P(\Lambda) = \frac{c}{A}\left(\Lambda - \frac{1}{\Lambda} + \Gamma\big(\Lambda^5 - \Lambda\big)\right).$$

6.12 Repeat the previous exercise for a Fung spherical membrane with $c > 0$, $c_1 = c_2$, and $c_1 + c_3 \equiv \Gamma > 0$.

6.13 Given the following dataset, use Eq. (6.50) to find best-fit values of the four material parameters; the units of the stress resultants are g/cm (convert them to N/m). [Data from Harris JL (2002) Thermal modification of collagen under biaxial isotonic loads. Ph.D. dissertation, Texas A&M University, College Station.]

Data points												
	1	2	3	4	5	6	7	8	9	10	11	12
T_1	1.0	1.2	1.3	1.6	2.4	4.9	6.6	8.5	10.5	13.0	15.0	16.8
Λ_1	1.44	1.44	1.44	1.44	1.44	1.43	1.43	1.43	1.43	1.43	1.44	1.44
T_2	1.0	1.3	1.7	2.6	5.4	14.8	23.8	32.0	42.6	52.1	64.5	73.2
Λ_2	1.06	1.12	1.19	1.26	1.33	1.40	1.41	1.43	1.43	1.43	1.44	1.44

6.14 Plot and compare the active stress–stretch response [Eq. (6.104)] for values of $T_0 = 0$, 20, 40, 60, and 80 kPa. Use values of $\Lambda_0 = 0.7$ and $\Lambda_m = 1.5$.

6.15 Repeat Exercise 6.14 with $T_0 = 50$ kPa and (Λ_0, Λ_m) pairs of (0.6, 1.3), (0.7, 1.4), and (0.8, 1.5) and discuss.

6.16 Given the proposed 1-D descriptor for smooth muscle behavior in arteries,

$$\sigma^a_{\theta\theta} = T_0\left(Ca^{2+}\right)\Lambda_\theta\left[1 - \left(\frac{\Lambda_m - \Lambda_\theta}{\Lambda_m - \Lambda_0}\right)^2\right],$$

where $T_0 \sim 50$ kPa in the basal state, Λ_m is the circumferential stretch at which activation is maximum ($\Lambda_m \sim 1.5$), and Λ_0 is that value of stretch at which active force generation ceases ($\Lambda_0 \sim 0.6$), add this contribution to the passive stress of Eq. (6.90) and recompute and plot the stress fields in Fig. 6.22. Note, too, that Λ_θ is simply the circumferential stretch and, thus, $\Lambda_\theta = \pi r/\Theta_0 R$.

6.17 P. Hunter, at Auckland New Zealand, proposed a different form of $T(\mathrm{Ca}^{2+}, \Lambda)$ for cardiac muscle. It is $T(\mathrm{Ca}^{2+}, \Lambda) = T_0(\mathrm{Ca}^{2+})f(\Lambda)$, where Λ is a stretch ratio for the sarcomere. Specifically, he let

$$T\left(\mathrm{Ca}^{2+}, \Lambda\right) = \left(\frac{[\mathrm{Ca}^{2+}]^n}{[\mathrm{Ca}^{2+}] + C_{50}^n}\right)T_{\max}[1 + \beta(\Lambda - 1)],$$

where

$$C_{50}^n = \frac{4.35}{\sqrt{e^{4.75(L-1.58)} - 1}}$$

and where L is the sarcomere length in μm (range from 1.58 to 2.2 μm), $n = 2$, $T_{\max} = 100$ kPa, $\beta = 1.45$, and $\Lambda = L/1.58$ μm. Plot and compare values of T for sarcomere lengths from 1.58 to 2.2 μm for two different calcium levels: 1.8 and 1.04 μM.

6.18 Using results from Exercise 6.17, compare the active stress generation (kPa) at a sarcomere length of 1.8 μm for all calcium concentrations from 1.04 μM to 1.8 μM; that is, plot T versus $[\mathrm{Ca}^{2+}]$.

6.19 The total axial force f on the artery is computed via

$$f = \int_0^{2\pi} \int_{r_l}^{r_a} \sigma_{zz} r dr d\theta.$$

Because of the Lagrange multiplier p, however, it proves useful to (do it) convert the integral to

$$f = \pi \int_{r_i}^{r_a} (2\sigma_{zz} - \sigma_{rr} - \sigma_{\theta\theta}) r dr - \pi r_i^2 \sigma_{rr}(r_i) + \pi r_a^2 \sigma_{rr}(r_a).$$

Hint: Let $\sigma_{zz} = \sigma_{zz} - \sigma_{rr} + \sigma_{rr}$, integrate by parts, and use the radial equilibrium equation

$$\frac{d\sigma_{rr}}{dr} + \frac{\sigma_{rr} - \sigma_{\theta\theta}}{r} = 0.$$

6.20 Find the components of $[C] = [A][B]$ if

$$[A] = \begin{bmatrix} A_{11} & A_{12} & A_{13} \\ A_{21} & A_{22} & A_{23} \\ A_{31} & A_{32} & A_{33} \end{bmatrix}, \quad [B] = \begin{bmatrix} B_{11} \\ B_{21} \\ B_{31} \end{bmatrix}.$$

6.21 If $[I]$ is the identity matrix, show that $[I][A] = [A] = [A][I]$.

6.22 If $[X]$ is a 3×1 matrix, we sometimes call it a column matrix or simply a vector. Noting from Eq. (A6.7) that $[X]^T[X]$ yields a scalar equal to the sum of the squares of the entries, compare this result to the vector dot product $\boldsymbol{X} \cdot \boldsymbol{X}$ if

$$\boldsymbol{X} = X_1 \hat{\boldsymbol{e}}_1 + X_2 \hat{\boldsymbol{e}}_2 + X_3 \hat{\boldsymbol{e}}_3.$$

We see, therefore, that operations in matrix methods can yield the same results as those in vector methods. Matrix methods are particularly well suited if m and/or n are >4 in a $m \times n$ matrix.

6.23 Show that $\det[A] = \det[A]^T$.

6.24 If

$$[A] = \begin{bmatrix} 2 & 4 & 2 \\ 2 & -1 & -2 \\ 4 & 1 & -2 \end{bmatrix},$$

show that

$$[A]^{-1} = \frac{1}{4}\begin{bmatrix} 4 & 10 & -6 \\ -4 & -12 & 8 \\ 6 & 14 & -10 \end{bmatrix},$$

and that $[A][A]^{-1} = [I]$.

6.25 In contrast to the neo-Hookean descriptor for rubber (Exercise 6.9), some prefer the Mooney-Rivlin relation. In terms of principal stretches, it is

$$W = C\left[\left(\Lambda_1^2 + \Lambda_2^2 + \Lambda_3^2 - 3\right) + \Gamma\left(\frac{1}{\Lambda_1^2} + \frac{1}{\Lambda_2^2} + \frac{1}{\Lambda_3^2} - 3\right)\right]$$

where C and Γ are material parameters. Recompute results in Fig. 6.15 for $\Gamma = 0.1$. See Humphrey (2002), Chap. 4.

6.26 Related to the discussion in Sect. 6.3, Humphrey et al. (1990) presented a solution for the finite deformation of a thin slab of excised passive myocardium that was motivated by the desire to identify a specific functional form of the requisite nonlinear constitutive relation directly from experimental data. Re-derive the basic equations that allow one, in principle, to determine the two associated "response functions" in terms of experimentally measurable quantities, including the applied loads, geometry, and deformations.

6.27 Whereas the discussion of torsion in Chap. 4 was restricted to linearly elastic responses over small strains, Humphrey et al. (1992) presented a solution for the finite extension and torsion of a papillary muscle from the heart (i.e., a cylindrical specimen). Re-derive the basic equations that allow one, in principle, to determine the two associated "response functions" in terms of experimentally measurable quantities, including the applied loads, geometry, and deformations. Contrast the difficulty of this analysis with that of problem 6.26. Finally, note that Criscione et al. (1999) extended this solution of Humphrey et al. to delineate effects due to the myocardium and endocardium that constitute a papillary muscle.

6.28 Simon et al. (2012) presented a novel finite deformation solution for a long-standing assay of cell—matrix interactions, the free-floating fibroblast-seeded collagen gel. Similar to the in-plane biaxial stretching problem discussed in Sect. 6.3, under some conditions it appears that the strain field may be homogeneous and equibiaxial and the stress field planar in this experiment. Reformulate this boundary value problem and reproduce the numerical findings presented in Figure 1 in Simon et al. Discuss the implications of the residual type stress field that is implicated.

6.29 Observation 3.1 introduces the topic of "stress concentrations," which typically result due to an abrupt change in geometry, material properties, or applied loads. The classical discussion of stress concentrations focuses on stresses at the edge of a hole, typically circular, within a thin plate that is subjected to uniform far field stresses. Associated stress concentration factors (i.e., values of maximum stress at the edge relative to the value of stress in the far field) are typically reported to be ~2–3. Whereas such results are usually based on linearized isotropic elasticity, David and Humphrey (2004) showed that stress concentration factors can be very different in cases of nonlinear elasticity and anisotropy. Re-derive the governing ordinary differential equation from David and Humphrey (2004) upon which these nonlinear results are based.

6.30 Atomic force microscopy (AFM) is discussed in Sect. 5.4.2 because one can use ideas from linear beam theory to design and calibrate the cantilevered-based probe, which typically experiences small strains during use. On the other hand, many investigators inappropriately use linearized elasticity to interpret the associated force—indentation data when using AFM to assess mechanical properties of cells or tissues. Re-derive the basic equations presented by Na et al. (2004), which are based on the theory of "small deformations superimposed on large" and thereby are better for interpreting such AFM data. Yet, because of the complexity involved in most AFM studies, inverse Finite Element Methods are probably best for data analysis.